Integrated entangling gates

Creating GHZ States for Stabilizer Measurements in Distributed Quantum Computing

Master's Thesis

Yorgos Sotiropoulos

Delft University of Technology

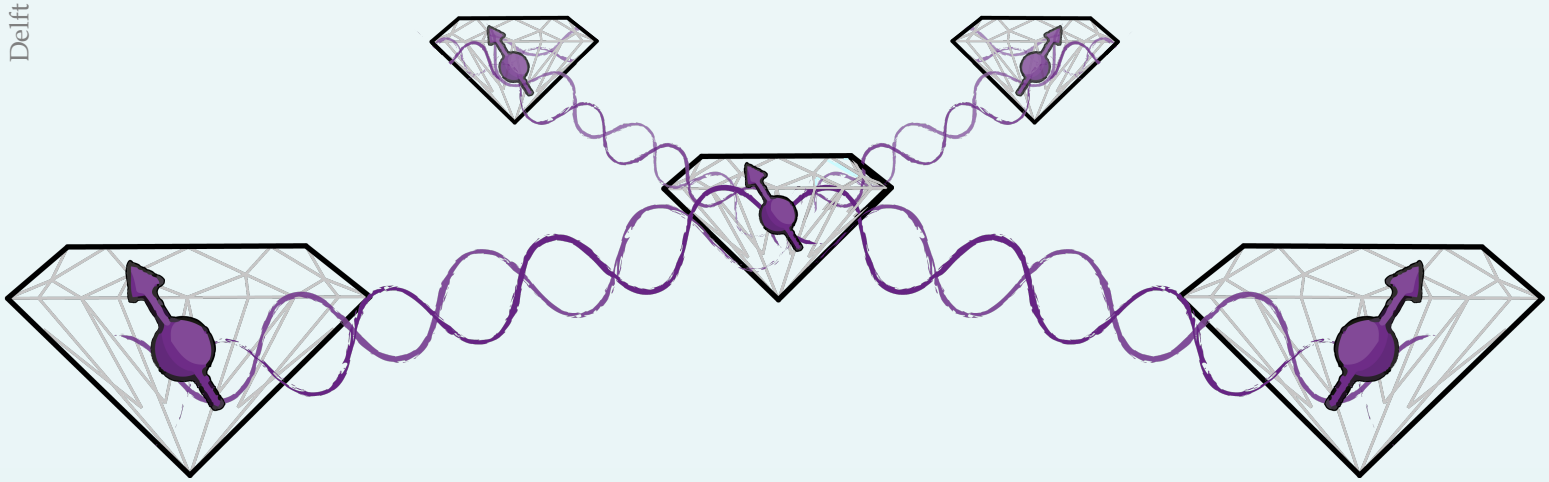

TU Delft

Integrated entangling gates

Creating GHZ States for Stabilizer Measurements in Distributed Quantum Computing

by

Yorgos Sotiropoulos

to obtain the degree of Master of Science
at the Delft University of Technology,
to be defended publicly on Monday June 13, 2022 at 13:00.

Student number:	5231175	
Project duration:	June 1, 2021 – May 27, 2022	
Thesis committee:	Prof. dr. Gary Steele,	TU Delft
	Prof. dr. David Elkouss,	TU Delft
	Prof. dr. Johannes Borregaard,	TU Delft, supervisor
Daily Supervision:	Fenglei Gu,	TU Delft, PhD student
	Sebastian de Bone,	TU Delft, PhD student

Cover:	Adapatation of picture in QuTech's blog: https://blog.qutech.nl/2018/11/26/how-can-we-speed-up-the-quantum-internet/
Style:	TU Delft Report Style, with modifications by Daan Zwaneveld

ONASSIS FOUNDATION

QuTech

TU Delft

Preface and Acknowledgements

The thesis report that lies before you is written in a way that I deemed suitable to address my fellow Master's students with a Quantum Computing background. To get the most out of it, it is very useful to be familiar with concepts from Cavity Electrodynamics and Quantum Error Correction. I tried to make my explanations as simple as I could, presenting the concepts in the way that I came to understand them. My goal was to make it comprehensible to my past self, before I took up this project.

This project builds on the vision of a distributed quantum computer. The main idea of this paradigm is to circumvent the problems caused by trying to pack together lots of qubits, as is the case with superconducting qubits. Instead, we can create a quantum computing device by linking together small autonomous quantum processing units of a few qubits, thus enabling scalability by mere addition of these units.

However, to achieve fault tolerance in these non-monolithic architectures, one has to have access to entangled states of high quality among the processing units. This a quite challenging task as the lapse of time is constantly endangering the delicate nature of quantum information. Thus, we are in need of mechanisms that will be able to generate entanglement links rapidly and with high fidelity.

This is where our project comes into play. We are investigating an expansion of an entangling protocol, initially designed for non-distributed architectures, but rather atoms in a single cavity. We expand it to distributed architectures with a powerful computational framework that we developed. This framework allowed for efficient and rapid analytical solutions that made our work plausible in this time window corresponding to 42 academic credits. Apart from that, it probably generated more questions than it answered which is something that I never expected.

I would like to thank the group of people without whom this work would not be possible. Fenglei and Sebastian, two PhD students that were my daily supervisors and were quick to help me at all times with the theoretical and numerical part of the project, respectively. I would like to thank my second supervisor (officially committee member) prof. David Elkouss for his contributions to the parts of Quantum Error Correction and being of crucial importance for setting our results in the bigger picture of distributed quantum computing. Lastly, I would like to thank my supervisor prof. Johannes Borregaard who came up with this project, brought together this amazing team and guided me insightfully throughout this challenging project.

I would also like to thank the Onassis foundation whose scholarship funded my studies in the Netherlands for these two years.

This report concludes my studies at TU Delft and I would like to thank all the people that I got to know, had fun with, and supported each other on the really cloudy days. In the order that I met you, thank you Smit, Luigi, Alberto, Matteo, Ina, Pol, Erica, Giulio, Matteo, Vicky, Klara, Juliette, Yiannis, Eli and Rob. I am grateful to have found you here.

Finally, I would like to thank my family for their ever present love.
Μάνα και πατέρα, σας ευχαριστώ.

Yorgos
Delft, May 2022

Abstract

High fidelity GHZ states among remote nodes is a precious commodity which can allow for non-local stabilizer measurements and thus pave the way for a modular fault-tolerant quantum computer [1]. To this end, we extend the high fidelity intracavity gate introduced by Borregaard et al. (2015) [2] to distributed paradigm, consisting of SnV-inspired atomic states in cavities connected by fibers. The adiabatic dynamics of this system can be solved efficiently using the effective operator formalism of Reiter and Sørensen (2012) [3]. We develop a Python framework that enables the analytical calculation of these effective dynamics reliably and swiftly, while being versatile and easily modifiable. The possibilities of this framework are showcased by obtaining results for a symmetric distributed setup and verifying its scalability. We present the ways that it can be optimized while taking into consideration experimentally inspired constraints, and proceed to optimize it for GHZ generation in color centers. These optimized gates are compared against an emission based protocol using the GHZ creation simulations of the Modicum protocol [4]. As a byproduct of our investigation, we identify a specific set of Hamiltonians which, under certain conditions, can generate GHZ states with a single multi-qubit entangling gate.

Contents

Nomenclature

Conventions and Abbreviations

- We will be assuming $\hbar = 1$. The only exception is section 2.1 for clarity. Thus, energy and frequency will be used interchangeably.
- **Bold** will be used in expressions to indicate vector quantities.
- Hats ˆ will be used to denote operators.
- h.c. in expressions is shorthand for "hermitian conjugate". For example:

$$\hat{H} = |0\rangle\langle 0| + a\left(b\,|0\rangle\langle 1| + \text{h.c.}\right)$$
$$\Leftrightarrow \hat{H} = |0\rangle\langle 0| + a\left(b\,|0\rangle\langle 1| + b^*\,|1\rangle\langle 0|\right).$$

- diag(a) is shorthand for a diagonal matrix with the elements of a in order.
- RWA stands for Rotating Wave Approximation
- EB stands for Emission Based
- NEB stands for Non-Emission Based

Protocol architecture symbols

Symbol	Definition	Number of States
0	Qubit atom in a cavity	6 atomic, 2 photonic
x	Auxiliary atom in a cavity	4 atomic, 2 photonic
-	Optical fiber	2 photonic

1

Introduction

The idea of using quantum mechanics as a means of computation was first introduced in 1982 by Richard Feynman [5]. Paul Benioff had already in 1980 and 1982 used quantum mechanical models to generalize the concept of a Turing machine [6, 7, 8]. Soon after, in 1985, David Deutsch conjectured that any physical process can be efficiently simulated using a universal machine [9]. This idea paved the way for the modern notion of quantum computation, given that we know that a big part of natural processes can be accurately described by quantum mechanics [10].

Before long, quantum circuits and quantum gates, equivalent to their classical binary counterparts, were defined and formulated in a comprehensive way [11, 12]. Quantum algorithms were designed that were able to complete certain tasks much more efficiently than the best performing classical algorithm. For example, Peter Shor in 1994 introduced a factoring algorithm which was consisting of a classical and quantum part that allowed for polynomial complexity, compared to the super-polynomial complexities of strictly classical algorithms [13]. Recently, the first instance of quantum supremacy was showcased experimentally using superconducting circuits to perform a task that would take a state-of-the-art classical supercomputer 10,000 years in an astonishing time of 200 seconds [14].

State-of-the-art implementations of quantum computers are quite diverse. Superconducting qubits, trapped ions, color centers and quantum dots are all viable options, each providing advantages and disadvantages against each other. One important theoretical basis for some of the above implementations is cavity electrodynamics, which will be at the heart of our exploration in this thesis.

Another way that quantum computing approaches are diversified is the centralization or not of the processing power of the quantum computer. Superconducting chips for example use transmon qubits, close to each other to form a single complex processing unit. Distinct characteristics of those are fast computation in exchange for potential cross talk noise among qubits. A distributed or modular quantum computer on the other hand consists of simple quantum computing units which are connected together to form a single quantum computing cluster [15, 16]. This distributed approach may not necessarily be implemented using remote nodes, though. In principle, it may be integrated on a single chip, but still holding the characteristics of the modular approach. These characteristics include restricted cross talk but at the expense of longer computational times.

Regardless of the physical implementation though, one vital, non-trivial milestone to conquer is quantum error correction. Quantum information in its core is fragile and delicate. Any minor imprecision, noise or even time elapsing cause quantum systems to dissipate information into the environment or interact among each other in ways that we cannot accurately predict or control. This, along with the fact that a general quantum state cannot be cloned [17], lead to the development of elaborate techniques to detect errors in quantum bits. These techniques depend on parity measurements rather than direct measurements of the qubits, which would collapse the quantum state [18]. One such instance is the surface code which assumes that the qubits are arranged on a two-dimensional square lattice [19].

In the case of modular quantum computers, parity measurements among remote nodes can be achieved by consuming shared entangled states known as GHZ states [20]. High fidelity GHZ states that can be obtained at a rapid pace is of paramount importance to this cause [1]. For that reason, it might be necessary to consider GHZ generating protocols that include distillation steps, which is the

process of consuming lower fidelity Bell pairs to generate entangled states with higher fidelity. The process of generating the GHZ state is a race against time due to the ever present decoherence.

The foundation stone of these entangled states is always an entangling protocol. This protocol will be used to generate Bell pairs that either have high fidelity, or can be obtained quickly or an appropriate combination of the two. This will allow the creation of high fidelity GHZ states to be efficient.

To this end, we propose a novel entangling gate to create Bell pairs in distributed architectures. This entangling gate is a generalization of the intra-cavity gate introduced by Borregaard et al. (2015) [2]. Its distinctive characteristics are that it uses weak external driving of an atom in a cavity as an architecture-integrated photon source. After the evolution, we measure this auxiliary atom and depending on the outcome, the success of the gate is determined. This probabilistic nature allows for high fidelity, as the measurement outcome heralds multiple error events.

The generalization entails distributing the atoms in different cavities connected by optical fibers. Moreover, the qubit atomic states are assumed to have additional couplings since in this way the modelling is closer to actual experimental implementations [21]. We use the effective operator formalism introduced by Reiter and Sørensen (2012) [3] to obtain the effective dynamics of the system in the adiabatic limit. Since the connectivity is not trivial, and we do not wish to restrict ourselves to specific assumptions, we developed a Python framework that calculates the analytical expressions of the effective dynamics. This allows for efficiency and easy introduction of any interaction or assumption, as well as any connectivity among the qubits and the auxiliary atom.

The original gate was shown to have performance error metrics that scale as $1/\sqrt{C}$ in the high cooperativity limit, thus making it scalable. After obtaining the effective dynamics of the gate, we find out that even by expanding the protocol, this scaling is preserved.

After verifying that this protocol has encouraging performance metrics, we proceed to optimize it for GHZ creation protocols. We define general parameters, hardware constraints and tunable parameters. The general parameters stay the same throughout, while the hardware constraints are selected to represent different experimental scenarios. For each given scenario, the gate is optimized such that it produces an appropriate combination of high fidelity and rapidly generated Bell pairs. This optimization takes place taking into consideration GHZ creation protocols hyperparameters.

The output of the optimization process is then used to demonstrate a proof of concept comparison between this protocol and an emission based protocol. This comparison is made based on the efficiency of the schemes in creating a 4-GHZ state following the Modicum protocol. To obtain these metrics, we use Monte Carlo simulations on the output density matrices of the entangling schemes.

Another avenue we explore is multi entangling qubit gates for direct GHZ state generation. We use the term quasi-symmetric setups to describe a general category of Hamiltonian interactions that can, under some conditions, generate a GHZ state using only one entangling unitary. We show that with a system of 4 atoms in two-sided cavities connected via fibers and using the proposed gate, we can generate a 3-GHZ state with a single entangling gate.

In chapter 2 we present some preliminaries, including the original gate. Next, in chapter 3 we present the generalization of the gate along with the theoretical exploration on quasi-symmetric setups. Chapter 4 contains our analytical and optimization results along with the optimization methods. Finally, we discuss and sum up our work in chapters 5 and 6.

2

Preliminaries

2.1. Basic Atomic Processes

Before we elaborate on the entangling protocol of this dissertation, we shall introduce briefly the description of some atomic processes. Note that whenever we refer to an *atom* in this thesis, we mean a multi-level quantum system which interacts with some electromagnetic field, classical or quantized. Also, we shall restrict ourselves to a very specific regime which is relevant for this dissertation. The following subsections are largely based on the Lectures of M.D. Lukin [22].

2.1.1. Interaction with classical field

Let us consider a nearly monochromatic electromagnetic field of the general form

$$\mathbf{E}(\mathbf{r},t) = \mathcal{E}(\mathbf{r},t)e^{-i(\nu t-\mathbf{k}\cdot\mathbf{r})} + \mathcal{E}(\mathbf{r},t)^* e^{i(\nu t-\mathbf{k}\cdot\mathbf{r})}. \tag{2.1.1}$$

If we assume that the field is weak and near the resonance frequency of an atomic transition, then the atom can be approximated by a two level system. [22, 23]. That is because the classical light-atom interaction can be considered a dipole oscillation driven by the light. Interactions with atomic transitions that are far from the frequency of the field ν will have small amplitudes. Thus, we can neglect them and only consider the resonant transition $|0\rangle \leftrightarrow |1\rangle$ to be of significance.

Let us also assume that the amplitude $\mathcal{E}(\mathbf{r},t)$ varies slowly temporally and spatially in comparison to the optical frequency ν and the wavelength $\frac{2\pi}{|\mathbf{k}|}$ respectively. Thus, we can neglect the spatial and temporal dependence of $\mathcal{E}$.

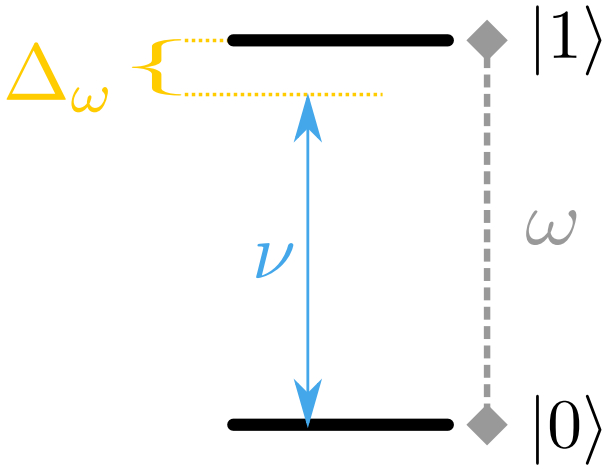

Figure 2.1: Interaction of electromagnetic field of frequency ν with two level system with energy splitting of $\hbar\omega$.

The interaction is described using the dipole operator $\hat{d} = e\hat{r}$ which for non an isolated atomic

system with rotational symmetry can be written as

$$\hat{d} = -\left(\mu \left|0\right\rangle \left\langle 1\right| + \mu^* \left|1\right\rangle \left\langle 0\right|\right), \tag{2.1.2}$$

where μ is the dipole moment for the transition $|0\rangle \leftrightarrow |1\rangle$ and the sign is selected to avoid negative signs in later expressions [23].

Note that the above expression also contains the hidden assumptions that only those two levels are relevant, and they do not exhibit permanent electric dipole properties, i.e. $\langle 1|\hat{d}|1\rangle = \langle 2|\hat{d}|2\rangle = 0$ [22].

The full Hamiltonian when energy level of state $|0\rangle$ is taken as 0 is

$$\hat{H}_{\text{full}} = \underbrace{\hbar\omega|1\rangle\langle 1|}_{\hat{H}_{\text{atom}}} + \underbrace{\left(\mu \left|0\right\rangle\!\left\langle 1\right| + \mu^* \left|1\right\rangle\!\left\langle 0\right|\right) \cdot \left(\mathcal{E}e^{ivt} + \mathcal{E}^* e^{-ivt}\right)}_{\hat{H}_{\text{int}}}. \tag{2.1.3}$$

The emerging quantity

$$\Omega = \frac{\mathcal{E}\mu}{\hbar} \tag{2.1.4}$$

is the so-called Rabi frequency [24] which is associated with the amplitude of the incoming field.

Switching to appropriate rotating frame Let us consider the rotating frame defined by the unitary

$$\hat{U} = e^{ivt|1\rangle\langle 1|} = e^{ivt} \left|1\right\rangle\!\left\langle 1\right| + \left|0\right\rangle\!\left\langle 0\right|. \tag{2.1.5}$$

Then, the Hamiltonian in the rotating frame [25] is given by

$$\hat{H}_{\text{R.F.}} = \hat{U}\hat{H}\hat{U}^\dagger + i\hbar\frac{d\hat{U}}{dt}\hat{U}^\dagger \tag{2.1.6}$$

$$\Rightarrow \hat{H}_{\text{R.F.}} = \hbar\Delta_\omega \left|1\right\rangle\!\left\langle 1\right| + \hbar\left(\left(\Omega + \frac{\mu\mathcal{E}^*}{\hbar}e^{-2ivt}\right)\left|0\right\rangle\!\left\langle 1\right| + \text{h.c.}\right), \tag{2.1.7}$$

where

$$\Delta_\omega = \omega - \nu. \tag{2.1.8}$$

Rotating wave approximation (RWA) Let the field be weak and near resonance [26, 24]:

$$\Omega \ll \nu \qquad \Delta_\omega \ll \nu, \omega. \tag{2.1.9}$$

Then, according to the rotating wave approximation we can disregard the term

$$\mu\mathcal{E}^* e^{-2ivt} \longrightarrow 0. \tag{2.1.10}$$

Intuitively, this can be understood as ignoring very fast oscillations in the presence of slower oscillations. This approximation is valid because over long period of time the effect of the Ω term will cause a slow oscillation between states 0 and 1 while the term $\mu\mathcal{E}^* e^{2ivt}/\hbar$ will be reversing itself with frequency $\nu \gg \Omega$, thus negating itself over this period [24].

Thus, under the RWA, the simplified Hamiltonian in the appropriate rotating frame is

$$\hat{H} = \hbar\Delta_\omega \left|1\right\rangle\!\left\langle 1\right| + \hbar\left(\Omega \left|0\right\rangle \left\langle 1\right| + \text{h.c.}\right), \tag{2.1.11}$$

which has no explicit time dependence.

2.1.2. Interaction with quantized electromagnetic field

Before we proceed to investigate the interaction of an atom, it is useful to discuss the quantization of the electromagnetic field, such that the notation and constraints of our approach are explicit.

Quantizing the electromagnetic field in vacuum
When charges and currents are not present, i.e. in a vacuum, Maxwell's equations can be condensed into [27]

$$\nabla^2 \mathbf{E} = \frac{1}{c^2}\frac{\partial^2 \mathbf{E}}{\partial^2 t}, \tag{2.1.12}$$

$$\nabla \times \mathbf{B} = \frac{1}{c^2}\frac{\partial \mathbf{E}}{\partial t}, \tag{2.1.13}$$

where eq. 2.1.12 is the wave equation for the electric field.

Considering that the field is restricted in a cavity of dimensions $L_x \times L_y \times L_z = V$. This leads to a set of allowed wavevectors $\mathbf{k}$ such that each component has [22]

$$k_{a,j} = \frac{2\pi}{L_a} j \qquad \text{with} \qquad a \in \{x, y, z\}\,,\ j \in Z^* \tag{2.1.14}$$

Note that each of those eigenmodes is composed of two orthogonal polarization modes for the field.

Using the generalized position $\mathbf{q}$, we can express a z-propagating and x-polarized electric field excitation as

$$E_x(z,t) = \sum_j A_j q_j(t) e^{ik_j z} \tag{2.1.15}$$

and, consequently

$$B_y = \frac{1}{c^2}\sum_j \frac{\dot{q}_j(t)}{k_j} A_j e^{ik_j z} \tag{2.1.16}$$

where A_j some normalization constant.

The Hamiltonian is according to classical electrodynamics

$$H = \frac{1}{2}\int dV \left(\epsilon_0 E^2 + \frac{1}{\mu_0}B^2\right) = \sum_j \frac{1}{2}A_j^2 \epsilon_0 V q_j^2 + \frac{1}{2}\frac{V}{c^4 \mu_0 k_j^2} A_j^2 \dot{q}_j^2. \tag{2.1.17}$$

Using that

$$c^2 = \frac{1}{\mu_0 \epsilon_0} \qquad \text{and} \qquad k_j = \frac{\nu_j}{c}, \tag{2.1.18}$$

we can make the selection

$$A_j = \sqrt{\frac{\nu_j^2}{V\epsilon_0}}, \tag{2.1.19}$$

such that we end up with the Hamiltonian

$$H = \sum_j \frac{\nu_j^2 q_j^2}{2} + \frac{\dot{q}_j^2}{2} \tag{2.1.20}$$

which is the Hamiltonian that also describes a set of harmonic oscillators with frequencies ν_j and mass equal to unity.

To quantize the field we shall turn the generalized coordinates into operators that satisfy the canonical commutational relation

$$[\hat{p}_l, \hat{q}_m] = i\hbar\delta_{l,m} \tag{2.1.21}$$

For each mode we can also define the creation and annihilation operators [22]

$$\hat{a}_j = \frac{1}{\sqrt{2\hbar\nu_j}}\left(\nu_j \hat{q}_j + i\hat{p}_j\right), \tag{2.1.22}$$

$$\hat{a}_j^\dagger = \frac{1}{\sqrt{2\hbar\nu_j}}\left(\nu_j \hat{q}_j - i\hat{p}_j\right), \tag{2.1.23}$$

such that

$$\hat{q}_j = \sqrt{\frac{\hbar}{2\nu_j}}\left(\hat{a}_j + \hat{a}_j^\dagger\right), \tag{2.1.24}$$

$$\hat{p}_j = -i\sqrt{\frac{\hbar\nu_j}{2}}\left(\hat{a}_j - \hat{a}_j^\dagger\right). \tag{2.1.25}$$

Thus, the Hamiltonian operator stemming from eq. 2.1.20 can be written as

$$\hat{H}_{\text{Q.F.}} = \sum_j \hbar\nu_j\left(\hat{a}_j^\dagger\hat{a}_j + \frac{1}{2}\right), \tag{2.1.26}$$

and the electric field operator will then be

$$\hat{\mathbf{E}}_\alpha = \varepsilon_\alpha \sum_j \sqrt{\frac{\hbar\nu_j}{\epsilon_0 V}}\frac{\left(\hat{a}_j e^{i\mathbf{k}_j\cdot\mathbf{r}} + \hat{a}_j^\dagger e^{-i\mathbf{k}_j\cdot\mathbf{r}}\right)}{\sqrt{2}}, \tag{2.1.27}$$

where ε_α the polarization unit vector.

Defining the positive frequency component

$$\hat{\mathcal{E}}_\alpha = \varepsilon_\alpha \sum_j \sqrt{\frac{\hbar\nu_j}{2\epsilon_0 V}}\hat{a}_j e^{i\mathbf{k}_j\cdot\mathbf{r}}, \tag{2.1.28}$$

we can rewrite the electric field operator as

$$\hat{E}_\alpha = \hat{\mathcal{E}}_\alpha + \hat{\mathcal{E}}_\alpha^\dagger. \tag{2.1.29}$$

Interaction Hamiltonian with atom

Similarly to the semi-classical approach in 2.1.1, the interaction Hamiltonian with an atom will be:

$$H_{int} = -\hat{d}\cdot\hat{\mathcal{E}}, \tag{2.1.30}$$

where $\hat{d}$ the dipole operator from equation 2.1.2.

Assuming that

- all interactions take place with the same polarization α
- only one transition $|0\rangle \leftrightarrow |1\rangle$ is significant which couples with a specific eigenfrequency ν which corresponds to a specific j
- transition $|0\rangle \leftrightarrow |1\rangle$ is not associated with a permanent electric dipole moment

we can write the interaction Hamiltonian as

$$H_{\text{int}} = \sqrt{\frac{\hbar\nu}{2\epsilon_0 V}}\left(\hat{a}e^{i\mathbf{k}\cdot\mathbf{r}} + \hat{a}^\dagger e^{-i\mathbf{k}\cdot\mathbf{r}}\right)\left(\mu\,|1\rangle\langle 0| + \mu^*\,|0\rangle\langle 1|\right). \tag{2.1.31}$$

Notice that the above expression is composed of terms that do not satisfy the conservation of energy. In particular, $\hat{a}\,|0\rangle\langle 1|$ corresponds to the atom decaying to state 0 while a photon is lost and its conjugate transpose $\hat{a}^\dagger\,|1\rangle\langle 0|$ to the inverse process. These terms analogously with the RWA approximation can be neglected [22].

Hence, we end up with the interaction Hamiltonian

$$\hat{H}_{\text{int}} = \hbar\left(g\,|0\rangle\langle 1|\,\hat{a}^\dagger + g^*\,|1\rangle\langle 0|\,\hat{a},\right) \tag{2.1.32}$$

where

$$g = \frac{\mu}{\hbar}\sqrt{\frac{\hbar\nu}{2\epsilon_0 V}} \tag{2.1.33}$$

is the *single-photon Rabi frequency*.

2.2. Adiabatic elimination via effective operator formalism

In this section we shall present the *Effective operator formalism for open quantum systems*, introduced by Reiter and Sørensen (2012) [3], which provides critical improvement in the efficiency of our calculations. It is a tool to facilitate adiabatic elimination in large open systems in a weak perturbative environment. To understand the importance of it, we need to first discuss adiabatic elimination itself.

2.2.1. Adiabatic elimination

When dealing with a small perturbation to our system, the first approach would be to simply neglect it. This is equivalent to assuming that the excited state associated with the perturbation is not initially populated and will remain so. However, this is a rather crude approximation which not only fails to capture the effect of the excited state, but also any other state that this excited state is coupled to [28].

A better approximation is made if instead of assuming that the population of the excited state is zero, we make the assumption that its rate of change is zero or at least insignificant with regard to the other parameters of the dynamics. This in turn simplifies greatly the equations of motion which may be solved analytically rather easily. For this to be valid, the excited state as mentioned earlier has to be weakly and off-resonantly coupled to the ground state. This leads to the so-called *elimination of the excited states* and an effective evolution on the ground state subspace which exhibits correction shifts as a first order correction due to these eliminated states.

This process which is already an appealing technique to approximate analytically complicated and potentially dissipative systems in the adiabatic regime, becomes efficient and elegant with the compact formalism proposed by Reiter and Sørensen (2012) [3]. Instead of having to express the state populations as a system of coupled differential equations of motion, we can easily obtain the effective Hamiltonian and Lindblad operators acting on the ground state subspace. The only significant computational hurdle is the inversion of a single matrix.

2.2.2. Effective operator formalism

Let there be a system that evolves under a Hamiltonian $\hat{H}$ in a dissipative environment described by a set of Lindblad operators $\hat{L}_k$.

The first step is to divide the Hamiltonian into the 4 terms

$$\hat{H} = \hat{H}_\mathrm{g} + \hat{H}_\mathrm{e} + \hat{V}_+ + \hat{V}_-, \tag{2.2.1}$$

where these terms encapsulate

- $\hat{H}_g$: ground state subspace interactions
- $\hat{H}_e$: excited state subspace interactions
- $\hat{V}_+$: weak interaction that excites ground states to excited states
- $\hat{V}_+$: weak interaction that de-excites excited states to ground states

Then, the effective Hamiltonian and Lindblad operators will be given by

$$\hat{H}_\mathrm{eff} = -\frac{1}{2}\hat{V}_- \left[\hat{H}_\mathrm{NH}^{-1} + \left(\hat{H}_\mathrm{NH}^{-1}\right)^\dagger\right]\hat{V}_+ + \hat{H}_\mathrm{g}, \tag{2.2.2}$$

$$\hat{L}_\mathrm{eff}^k = \hat{L}_k \hat{H}_\mathrm{NH}^{-1}\hat{V}_+, \tag{2.2.3}$$

where

$$\hat{H}_\mathrm{NH} = \hat{H}_\mathrm{e} - \frac{i}{2}\sum_k \hat{L}_k^\dagger \hat{L}_k \tag{2.2.4}$$

is the non-Hermitian Hamiltonian in the quantum-jump formalism introduced for the Monte-Carlo wave-function method by Mølmer, Castin, and Dalibard (1993) [29].

After this trivial linear algebra manipulation, we can extract the evolution as the solution of the Gorini–Kossakowski–Sudarshan–Lindblad equation or Lindblad master equation [30, 31]

$$\dot{\rho} = -i\left[\hat{H}_\mathrm{eff}, \rho\right] + \sum_k \hat{L}_\mathrm{eff}^k \rho \left(\hat{L}_\mathrm{eff}^k\right)^\dagger - \frac{1}{2}\left[\left(\hat{L}_\mathrm{eff}^k\right)^\dagger \hat{L}_\mathrm{eff}^k \rho + \rho\left(\hat{L}_\mathrm{eff}^k\right)^\dagger \hat{L}_\mathrm{eff}^k\right], \tag{2.2.5}$$

which describes the density matrix evolution in a dissipative environment. Notice how H_{eff} and $\hat{L}^k_{\text{eff}}$ act now on the ground state subspace and thus the evolution of the density matrix ρ does not involve the excited subspace [3].

2.3. Entangling protocol among atoms in a cavity with integrated error detection

In this section, we shall present the protocol which the entangling scheme of this thesis is an expansion of. It was introduced in Borregaard et al. (2015) [2], and it is capable of realizing a high fidelity N-Toffoli gate among N qubit atoms in a cavity. Its distinctive characteristic is the use of an extra auxiliary atom which acts both as an integrated photon emitter and as a means of error detection. We shall begin with a description of the dynamics while focusing only on the $N = 2$ case where a CZ gate is realized.

2.3.1. Protocol description

The auxiliary atom (see Fig.2.2a) consists of two metastable states $|g\rangle, |f\rangle$ and an excited state $|E\rangle$. It is externally driven by a weak classical electromagnetic field whose frequency ω_L is close to the frequency corresponding to the transition $|E\rangle \leftrightarrow |g\rangle$, with their difference being a detuning Δ_E. The transition $|E\rangle \leftrightarrow |f\rangle$ couples to some cavity mode, with the same detuning Δ_E[1]. The excited state decays to the ground states via spontaneous emission with rates γ_g and γ_f.

The qubit atom (see Fig.2.2b) consists of two ground states $|0\rangle, |1\rangle$, an excited state $|e\rangle$ and a decayed state $|\tilde{o}\rangle$. The transition $|e\rangle \leftrightarrow |g\rangle$ couples to the same cavity mode that is coupled to the auxiliary atom transition $|E\rangle \leftrightarrow |f\rangle$, with a detuning Δ_e. The excited state decays to the decayed state via spontaneous emission with a rate γ.

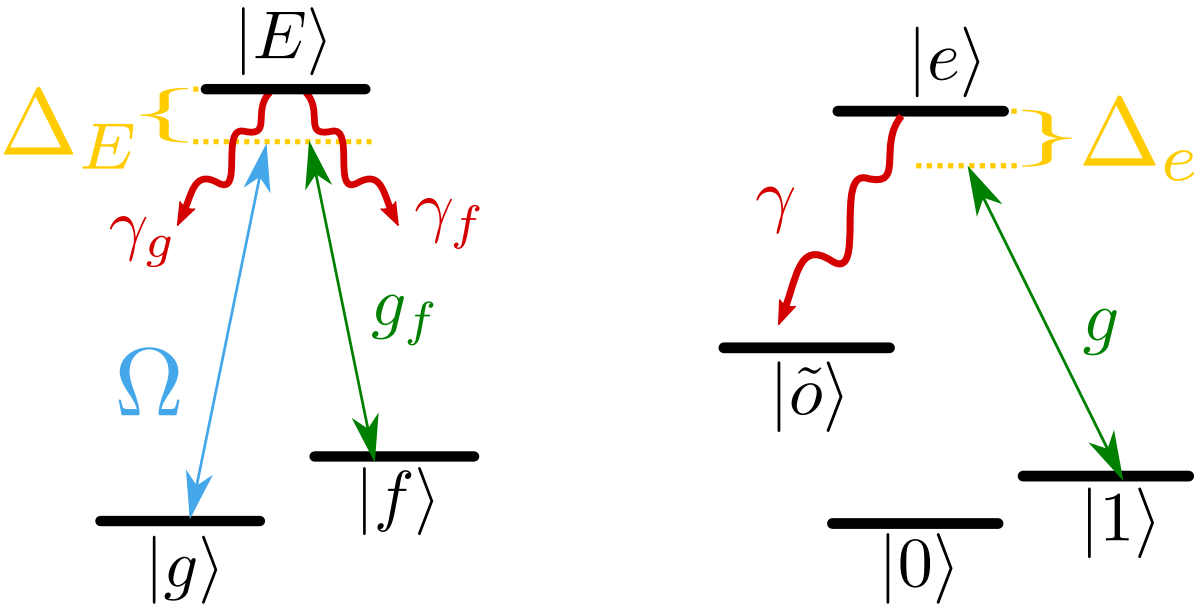

(a) Auxiliary atom levels and interactions. States $|g\rangle$ and $|f\rangle$ are metastable states while $|E\rangle$ is an excited state. The cavity couples with the transition $|E\rangle \leftrightarrow |f\rangle$ and the classical field Ω with the transition $|E\rangle \leftrightarrow |g\rangle$). The excited state decays to g and f with spontaneous emission rates γ_g and γ_f respectively.

(b) Qubit atom levels and interactions. States $|0\rangle$ and $|1\rangle$ are the ground states while $|e\rangle$ is an excited state. The cavity couples to the transition $|e\rangle \leftrightarrow |1\rangle$ and the excited state decays to some irrelevant level $|\tilde{o}\rangle$ with a spontaneous emission rate γ.

Figure 2.2: The protocol along with their losses via spontaneous emission and their interactions with the cavity and the classical field.

The bare Hamiltonian is

$$\hat{H}_{\text{bare}} = \hat{H}_{\text{aux}} + \hat{H}_{\text{qubits}} + \hat{H}_{\text{cavity}}. \tag{2.3.1}$$

[1]This means that the cavity is on resonance as we shall see later on.

In the RWA, using the results of section 2.1 and neglecting the constant energy of the vacuum and of all other modes that do not interact with the atomic transitions, we obtain in the appropriate rotating frame

$$\hat{H} = \Delta_E|E\rangle\langle E| + g_f(\hat{a}|E\rangle\langle f| + \text{ h.c. }) + \left(\Omega|E\rangle\langle g| + \text{ h.c. }\right) + \sum_{k=0}^{N-1} \Delta_e|e\rangle_k\langle e| + g\left(\hat{a}|e\rangle_k\langle 1| + \text{ h.c. }\right), \quad (2.3.2)$$

where k labels the qubit atoms. An extensive derivation of it is omitted since we shall be treating a more general case in the next chapter.

The detunings are

$$\Delta_E = \omega_E - \omega_g - \omega_L, \quad (2.3.3)$$
$$\Delta_e = \omega_e - \omega_g - \omega_L + \omega_f - \omega_1, \quad (2.3.4)$$

where ω_x the energy associated with level x.

The cavity mode is such that the transition $|g\rangle \leftarrow |E\rangle \leftarrow |f\rangle$ is a two-photon transition, i.e.:

$$\delta_c = \omega_c + \omega_f - \omega_g - \omega_L = 0 \quad (2.3.5)$$

or equivalently, the frequency of the cavity mode is

$$\omega_c = \omega_g + \omega_L - \omega_f, \quad (2.3.6)$$

such that the term

$$\hat{H}_{\text{cavity}} = \omega_c\hat{a}\hat{a}^\dagger \quad (2.3.7)$$

of the cavity field is eliminated in the rotating frame.

The dissipation in this system is described by the Lindblad operators

$$\hat{L}_c = \sqrt{\kappa_c}\hat{a} \quad (2.3.8)$$

for photon loss of the cavity, and

$$\hat{L}_f = \sqrt{\gamma_f}\,|f\rangle\langle E|, \quad (2.3.9)$$
$$\hat{L}_g = \sqrt{\gamma_g}\,|g\rangle\langle E|, \quad (2.3.10)$$
$$\hat{L}_k = \sqrt{\gamma}\,|\tilde{o}\rangle\langle e|, \quad (2.3.11)$$

for the decay from the excited states.

Assuming vacuum and $|g\rangle$ initialization, we can define the subspaces as follows:

- Ground state subspace spanned by:

$$|g\rangle \otimes \left\{ |00\rangle, |01\rangle, |10\rangle, |11\rangle \right\} \otimes |0_p\rangle \quad (2.3.12)$$

  of dimension $D_g = 4$.
- Excited state subspace spanned by:

$$\begin{aligned} &|E\rangle \otimes \left\{ |00\rangle, |01\rangle, |10\rangle, |11\rangle \right\} \otimes |0_p\rangle, \\ &|f\rangle \otimes \left\{ |00\rangle, |01\rangle, |10\rangle, |11\rangle \right\} \otimes |1_p\rangle, \\ &|f\rangle \otimes \left\{ |0e\rangle, |e1\rangle, |1e\rangle, |e1\rangle \right\} \otimes |0_p\rangle, \\ &|f\rangle \otimes \left\{ |0\tilde{o}\rangle, |\tilde{o}0\rangle, |1\tilde{o}\rangle, |\tilde{o}1\rangle \right\} \otimes |0_p\rangle \end{aligned} \quad (2.3.13)$$

  of dimension $D_e = 16$.

The Hamiltonian in the rotating frame of equation 2.3.2 can be treated with the effective operator formalism discussed in 2.2. This is possible so long as the effective driving to the excited state $\left|f\right\rangle \otimes \left|1_{\text{ph}}\right\rangle$ is much smaller than the decay rate κ_c of the excited state, i.e.

$$\frac{\Omega\, g_f}{\Delta_E} \ll \kappa_c. \tag{2.3.14}$$

This condition ensures that the driving is appropriately weak and off resonant. Simultaneously, it ensures that the probability of measuring non-zero cavity photons is negligible and therefore states with more than 0 cavity photons can be adiabaticly eliminated.

The effective Hamiltonian after the adiabatic elimination is thus projected on the ground state subspace

$$\hat{H}_{\text{eff}} = |g\rangle\langle g| \sum_n \Delta_n \hat{P}_n, \tag{2.3.15}$$

where

$$\Delta_n = -\frac{\Omega^2}{4\gamma}\,\text{Re}\left\{\frac{\left[\left(\frac{\Delta_e}{\gamma} - i/2\right) i + 2nC\right]}{\left(2\frac{\Delta_e}{\gamma} - i\right)\left[\left(2\frac{\Delta_E}{\gamma} - i\right) i/4 + C_f\right] + \left(2\frac{\Delta_E}{\gamma} - i\right) nC}\right\}. \tag{2.3.16}$$

$$C_{(f)} = \frac{g_{(f)}^2}{\kappa_c \gamma} \tag{2.3.17}$$

is the *atom-cavity cooperativity* and n represents the number of atoms in state $|1\rangle$. $\hat{P}_n$ is the sum of all the projectors with n atoms in state $|1\rangle$. More explicitly:

$$\hat{P}_0 = |00\rangle\langle 00|\,, \qquad \hat{P}_1 = |01\rangle\langle 01| + |10\rangle\langle 10|\,, \qquad \hat{P}_2 = |11\rangle\langle 11|\,. \tag{2.3.18}$$

Integrated error detection Similarly to the effective Hamiltonian, the effective Lindblad operators can be calculated. All of them, except for $\hat{L}_g$, cause the state of the system to be at a subspace which leaves the auxiliary atom in state $\left|f\right\rangle$. Because this subspace is out of the space on which the effective Hamiltonian or the Lindblad operators act, this will cause the auxiliary atom to be trapped in this state $\left|f\right\rangle$. After the evolution, we shall measure the auxiliary atom and, with some probability it will be found in $\left|g\right\rangle$, therefore eliminating the possibility of the these losses occurring. This will lead to an improvement in fidelity in exchange for some probability of failure, which failure is equivalent to measuring the auxiliary atom in the $\left|f\right\rangle$ state.

We shall refer to the errors occurring via $\hat{L}_g$ as *undetectable* since they directly impact the fidelity of the resulting state. The rest of the errors will be referred to as *detectable* as we can identify their occurrence by measuring the auxiliary atom as discussed previously.

The probability of success will be the probability that the final density matrix ρ_f is in the ground state subspace

$$P_{\text{success}} = \text{Tr}[\rho_f |g\rangle\langle g|]_e, \tag{2.3.19}$$

where the trace is taken on the excited subspace, resulting in the density matrix

$$\rho_{f,\text{ground}} = \frac{|g\rangle\langle g|\rho_f|g\rangle\langle g|}{P_{success}}. \tag{2.3.20}$$

2.3.2. Generating a CZ gate

The unitary generated by the Hamiltonian will be:

$$\hat{U}(t) = e^{-i\hat{H}_{\text{eff}}t}. \tag{2.3.21}$$

Since $\hat{H}_{eff}$ is diagonal, $\hat{U}$ can be written for a scheme with 2 qubit atoms and 1 auxiliary atom in the cavity as

$$U(t) = \sum_{n=0}^{2} e^{-i\Delta_n t} \left|g\right\rangle\!\left\langle g\right| \otimes \hat{P}_n, \tag{2.3.22}$$

While exploring the possibilities of this unitary we have to keep in mind two parameters:

- The resulting unitary need not be exactly what we want it to be, but it suffices to be the same up to some *global phase*.
- The resulting unitary can still be of value if it can be corrected into a particular unitary through *single qubit rotations*, since these can often be executed quickly and with high fidelity.

Thus, the desired gate has to be able to be expressed as:

$$\hat{U}_{\text{target}} = e^{i\alpha} R(\boldsymbol{\theta}) U(t) \tag{2.3.23}$$

for some combination of the parameters where $R(\boldsymbol{\theta})$ represents a tensor product of single qubit unitary gates.

To implement a CZ gate, the target unitary is:

$$U_{\text{target}} = \text{diag}(1, 1, , 1, -1) \tag{2.3.24}$$

Manipulating the total unitary for single qubit arbitrary rotations over the Z axis:

$$\begin{aligned} R_z(\theta_1, \theta_2)\, U(t) &= \text{diag}\left(1, e^{i\theta_1}, e^{i\theta_2}, e^{i(\theta_1+\theta_2)}\right) \text{diag}\left(e^{-i\Delta_0 t}, e^{-i\Delta_1 t}, e^{-i\Delta_1 t}, e^{-i\Delta_2 t}\right) \\ &= e^{-i\Delta_0 t}\, \text{diag}(1, e^{i[\theta_1-(\Delta_1-\Delta_0)t]}, e^{i[\theta_2-(\Delta_1-\Delta_0)t]}, e^{i[\theta_1+\theta_2-(\Delta_2-\Delta_0)t]}\Big) \end{aligned} \tag{2.3.25}$$

Selecting:

$$\theta_1 = (\Delta_1 - \Delta_0)\, t \tag{2.3.26}$$

$$\theta_2 = (\Delta_1 - \Delta_0)\, t \tag{2.3.27}$$

$$(\Delta_0 - \Delta_2)t + \theta_1 + \theta_2 = \pi \tag{2.3.28}$$

The unitary is equivalent to a CZ gate up to a global phase. The gate time then becomes:

$$t_g = \frac{\pi}{|\Delta_0 + \Delta_2 - 2\Delta_1|} \tag{2.3.29}$$

while the correcting rotation angles are:

$$\theta_1 = \frac{\Delta_0 - \Delta_1}{|\Delta_0 + \Delta_2 - 2\Delta_1|}\, \pi \tag{2.3.30}$$

$$\theta_2 = \frac{\Delta_0 - \Delta_1}{|\Delta_0 + \Delta_2 - 2\Delta_1|}\, \pi \tag{2.3.31}$$

2.3.3. Parameter selection of the scheme

Previously, we glossed over our claim that the fidelity can be greatly increased due to the possibility of detecting all but one kind of errors. However, this still has restrictions that one has to consider. Let us consider the detectable errors represented by the effective Lindblad operators $\hat{L}^{\text{eff}}_{\text{det},i}$ and no undetectable errors, i.e.

$$\hat{L}^{\text{eff}}_{g} = 0, \tag{2.3.32}$$

as these can be mitigated by means of two photon driving, which we shall not be delving into.

Equating the detectable losses

Since we only proceed with the scheme if we measure the auxiliary atom in the $|f\rangle$ state, the output density matrix of the evolution will be given by the partial trace [10] over all states with the auxiliary atom in $|f\rangle$. The detectable losses would lead to a decay rate of the ground states which can be described by the non-Hermitian Hamiltonian evolution from equation 2.2.4

$$\hat{H}_{\text{NH}} = \hat{H}_{\text{eff}} - \frac{i}{2} \sum_j \left(\hat{L}^{\text{eff}}_{\text{det},j}\right)^{\dagger} \hat{L}^{\text{eff}}_{\text{det},j}, \tag{2.3.33}$$

which acts on the ground state subspace.

This will lead to the dissipative evolution

$$\begin{aligned}\hat{U}_{\text{dis}} &= e^{-i\hat{H}_{\text{NH}}} \\ &= \text{diag}\left(e^{-i\Delta_0 t-\Gamma_0 t/2}, e^{-i\Delta_1 t-\Gamma_1 t/2}, e^{-i\Delta_1 t-\Gamma_1 t/2}, e^{-i\Delta_2 t-\Gamma_2 t/2}\right),\end{aligned} \tag{2.3.34}$$

where

$$\Gamma_0 = \sum_j \langle 00|\left(\hat{L}^{\text{eff}}_{\text{det},j}\right)^\dagger \hat{L}^{\text{eff}}_{\text{det},j}|00\rangle \tag{2.3.35}$$

$$\begin{aligned}\Gamma_1 &= \sum_j \langle 01|\left(\hat{L}^{\text{eff}}_{\text{det},j}\right)^\dagger \hat{L}^{\text{eff}}_{\text{det},j}|01\rangle \\ &= \frac{1}{2}\sum_j \langle 10|\left(\hat{L}^{\text{eff}}_{\text{det},j}\right)^\dagger \hat{L}^{\text{eff}}_{\text{det},j}|10\rangle\end{aligned} \tag{2.3.36}$$

$$\Gamma_2 = \sum_j \langle 11|\left(\hat{L}^{\text{eff}}_{\text{det},j}\right)^\dagger \hat{L}^{\text{eff}}_{\text{det},j}|11\rangle \tag{2.3.37}$$

is the total loss rate out of each state of the ground state subspace.

Assuming we initialize the qubits in state

$$\left|\psi_i\right\rangle = |{+}{+}\rangle = \frac{1}{2}\left(|00\rangle + |01\rangle + |10\rangle + |11\rangle\right), \tag{2.3.38}$$

the final non-normalized state will be

$$\left|\psi_{out}\right\rangle = \frac{1}{2}\left(e^{-i\Delta_0 t-\Gamma_0 t/2}|00\rangle + e^{-i\Delta_1 t-\Gamma_1 t/2}|01\rangle + e^{-i\Delta_1 t-\Gamma_1 t/2}|10\rangle + e^{-i\Delta_2 t-\Gamma_2 t/2}|11\rangle.\right) \tag{2.3.39}$$

Assuming success, whose probability is the normalization factor

$$P_s = \frac{e^{-\Gamma_0 t} + e^{-\Gamma_2 t} + 2e^{-\Gamma_1 t}}{4}, \tag{2.3.40}$$

we end up with the final state

$$\left|\psi_{out}\right\rangle = \frac{1}{\sqrt{P_s}}\left(e^{-i\Delta_0 t-\Gamma_0 t/2}|00\rangle + e^{-i\Delta_1 t-\Gamma_1 t/2}|01\rangle + e^{-i\Delta_1 t-\Gamma_1 t/2}|10\rangle + e^{-i\Delta_2 t-\Gamma_2 t/2}|11\rangle\right). \tag{2.3.41}$$

It is clear that in the general case where

$$\Gamma_0 \neq \Gamma_1 \neq \Gamma_2, \tag{2.3.42}$$

the final state after the post-gate rotations will be

$$\left|\psi_f\right\rangle \neq \frac{1}{2}\left(|00\rangle + |01\rangle + |10\rangle + -|11\rangle\right). \tag{2.3.43}$$

assuming the selections made in equations 2.3.26-2.3.28. The fidelity of the final state will thus be impaired, and the total evolution will not be a CZ gate. Intuitively, this can be understood as information leaking due to this asymmetrical decaying of the states. A "success" measurement of the auxiliary atom in these cases, provides us with information about the state of the system. Thus, the fidelity is compromised.

However, we can select the detunings such that the losses Γ_k are all equal among themselves. Writing out the expressions for the losses, one can see that this can be achieved by choosing

$$\Delta_E = \frac{\gamma}{2}\sqrt{\beta}\sqrt{4\alpha C + \beta}, \tag{2.3.44}$$

$$\Delta_e = \frac{\alpha C \gamma^2}{2\Delta_E}, \tag{2.3.45}$$

where

$$\alpha = \frac{C_f}{C}, \tag{2.3.46}$$

$$\beta = \frac{\gamma_f}{\gamma}. \tag{2.3.47}$$

This leads to a perfect output fidelity, if $\gamma_g = 0$.

Preserving the perturbative regime
All of our derivations are based on the assumption that we can treat the driving as a perturbation of the system. This means that the driving strength Ω have to be in accordance to equation 2.3.14. Assuming that

$$g \ll \kappa_c \Rightarrow C \ll \frac{\kappa_c}{\gamma} \tag{2.3.48}$$

equation 2.3.14 can be rewritten as

$$\Omega \ll \Delta_E \sim \gamma\sqrt{C}. \tag{2.3.49}$$

So, we can select

$$\Omega = \epsilon\gamma\sqrt{C}, \tag{2.3.50}$$

with ϵ such that 2.3.49 is satisfied.

Scaling of the scheme
The previous selection of the detunings has a dual purpose, though. Apart from equating the losses and eliminating fidelity losses, it also allows the gate to improve its performance as the cooperativity increases. In particular, in the high cooperativity limit $C \gg 1$ it turns out that

$$t_g \approx \frac{\pi\sqrt{\alpha}(\alpha + 2\beta)(\alpha + 4\beta)}{2\beta^{3/2}\epsilon^2}\frac{1}{\gamma\sqrt{C}}, \tag{2.3.51}$$

$$P_{fail} \approx \pi\frac{8\beta^2 + 6\beta\alpha + \alpha^2}{8\beta^{3/2}\sqrt{\alpha}}\frac{1}{\sqrt{C}}. \tag{2.3.52}$$

We can see that the higher the cooperativity, the faster the gate will be and the less the probability of failure will be. Note that the cooperativity is a measure of how strong is the cavity coupling compared to the photon loss rate of the cavity and the decaying of the excited state to the ground state, and as a result it is a measure of how well the experimental setup works. With such a scaling, we expect this protocol to perform better and better as the optical setup improves in terms of coupling and losses.

2.4. Quantum Error Correction

Quantum information, just like its classical counterpart needs to be resilient to errors in order for computation to be possible. However, quantum information has the peculiarity that it cannot be duplicated, since in general a quantum state cannot be cloned, according to the *No-Cloning Theorem* by Wootters and Zurek (1982) [17]. As a result, more sophisticated methods have been developed to preserve quantum information despite lossy channels, which may be due to the qubits physically moving in space or time just elapsing.

The basic idea behind quantum error correction is to encode a collection of physical qubits into fewer or a single logical qubit. This way, the logical qubit will be able to be decoded into the initial logical state as long as the physical errors do not exceed some threshold. Effectively, this means that redundancy is added to the system by means of expanding the Hilbert space [32]. Encoding k qubits using n physical qubits will lead to 2^k basis logical states/codewords in the Hilbert space of dimension 2^n. Any linear combination of logical states shall also be a logical state. Hence, any k qubit state can be represented as a logical state.

2.4.1. Stabilizers

Over many lossy channels the efficiency of the error correcting code will be impaired due to error accumulation. Thus, arises the need to identify errors and correct them periodically through the so-called *error correcting cycles*. To this end, non-destructive measurements should be performed on the encoded state to detect errors [33]. Auxiliary qubits need to be used for this so that these projective measurements may take place. Such measurements are the *stabilizer* measurements [34] and are part of a stabilizer group S.

A stabilizer $\hat{M}_i \in S$ should satisfy

$$\hat{M}_i \left|\psi\right\rangle_L = \left|\psi\right\rangle_L, \quad \forall \left|\psi\right\rangle_L \in T, \tag{2.4.1}$$

where $\left|\psi\right\rangle_L$ a logical state and T the *coding space* [18].

Moreover, all the stabilizers should commute with each other such that they can be measured simultaneously, and their order is irrelevant

$$\left[\hat{M}_i, \hat{M}_j\right] = 0, \quad \forall \hat{M}_i, \hat{M}_j \in S. \tag{2.4.2}$$

The utility of the stabilizers becomes apparent by the fact that each of them anti-commutes with the elements $\hat{E}_j$ of a subset of possible single qubit errors $\mathscr{E}_i$, i.e.

$$\left\{\hat{E}_i, \hat{M}_i\right\} = 0, \quad \hat{E}_j \in \mathscr{E}_i. \tag{2.4.3}$$

This means that if a number of these errors occur, then the expected value of the stabilizer $\hat{M}_i$ will be

$$\left\langle \hat{M}_i \right\rangle = \left\langle \psi_e \right| \hat{M}_i \left| \psi_e \right\rangle \tag{2.4.4}$$

where

$$\left|\psi_e\right\rangle = \prod_j \left(E_j\right) \left|\psi\right\rangle_L. \tag{2.4.5}$$

We can commute $\hat{M}_i$ through all the errors accumulating a -1 sign for every commutation according to the relation 2.4.3. Thus, the resulting expectation value will be

$$\left\langle \hat{M}_i \right\rangle = \begin{cases} 1 & \text{if number of errors is odd,} \\ -1 & \text{if number of errors is even or zero.} \end{cases} \tag{2.4.6}$$

If the error probability is low enough, then we can interpret the stabilizer measurement $\hat{M}_i$ as an indication of whether a single qubit error of the set $\mathscr{E}_i$ occurred. That is because events with two errors or more will be unlikely.

2.4.2. The Surface Code

One of the many promising error correcting codes for quantum information is the *planar surface code*[19] which is a variant of the *toric surface code*, introduced by Kitaev [35, 36]. This error correcting code is designed with the assumption that the data and auxiliary qubits are arranged in a two-dimensional lattice. By data qubits we refer to the qubits containing the logical state while auxiliary will be the qubits used to measure the stabilizers of the code.

For a square lattice, the surface code depends on measuring two kinds of stabilizers among 4 data qubits in proximity [33]. The so-called *plaquette* stabilizers

$$\hat{M}_{\text{plaq},i} = \prod_{j \in \left\{ \begin{smallmatrix} \text{4 data qubits} \\ \text{around plaquette } i \end{smallmatrix} \right\}} Z_j, \tag{2.4.7}$$

and the *star* stabilizers

$$\hat{M}_{\text{star},i} = \prod_{j \in \left\{ \begin{smallmatrix} \text{4 data qubits} \\ \text{around vertex } i \end{smallmatrix} \right\}} X_j. \tag{2.4.8}$$

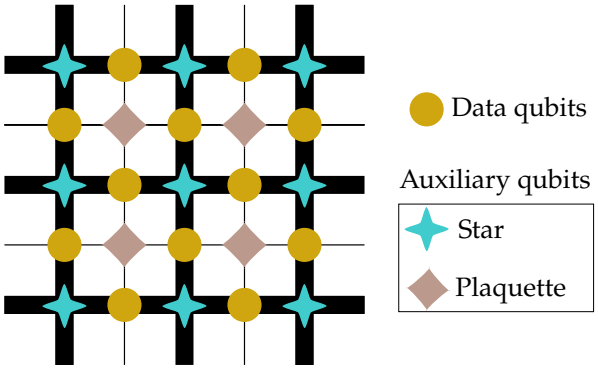

Figure 2.3: Sketch of the surface code lattice on a monolithic architecture.

The combination of those are able to detect any arbitrary Pauli error [37] as

$$\left\{\hat{X},\hat{Z}\right\} = \left\{\hat{Y},\hat{Z}\right\} = \left\{\hat{X},\hat{Y}\right\} = 0. \tag{2.4.9}$$

An X error on a data qubit will cause the plaquette stabilizer measurement to be measured -1 by the four nearby auxiliary-plaquette qubits. A Z error will act similarly on the nearby star stabilizer measurements and a Y error will act on both. Consequently, if the lattice does not suffer too many Pauli errors, then it may be possible to identify them correctly and restore the logical state.

2.4.3. Non-local stabilizer measurements

Let us revisit the surface code on a square lattice but now with a different approach. Instead of using the star and plaquette auxiliary qubits of the lattice, we shall assume that the data qubits are stations that apart from the data qubit, the also have auxiliary qubits. These stations share a 4-GHZ state [20] for every stabilizer measurement that needs to be performed, stored using the auxiliary qubits. We shall show that by consuming the GHZ state, it is possible to measure the necessary stabilizers.

In general, an N-GHZ state is of the form

$$|\mathrm{GHZ}\rangle_N = \frac{1}{\sqrt{2}}\left(|0\rangle^{\otimes N} + |1\rangle^{\otimes N}\right), \tag{2.4.10}$$

and thus for the square lattice

$$|\mathrm{GHZ}\rangle = \frac{1}{\sqrt{2}}\left(|0000\rangle + |1111\rangle\right). \tag{2.4.11}$$

By applying the plaquette stabilizer circuit between the 4 data qubits in state $|\psi_4\rangle$ and the 4 auxiliary atoms in the GHZ state [33]

$$|\Psi_s\rangle = \frac{1}{\sqrt{2}}\left(|0000\rangle \otimes \hat{I}^{\otimes 4} + |1111\rangle \otimes \hat{Z}^{\otimes 4}\right)|\psi_4\rangle \tag{2.4.12}$$

where the $\hat{I}^{\otimes 4}, \hat{Z}^{\otimes 4}$operators act on all 4 data qubits.

Measuring in the X basis, which is equivalent to applying a Hadamard gate, gives

$$\begin{aligned}
|\Psi_{stab}\rangle &= H^{\otimes 4} \otimes I^{\otimes 4} |\Psi_s\rangle \\
&= \frac{1}{4\sqrt{2}} \left(|+++\rangle \otimes \hat{I}^{\otimes 4} + |---\rangle \otimes \hat{Z}^{\otimes 4} \right) |\psi_4\rangle \\
&= \frac{1}{4\sqrt{2}} \left(\sum_x^{2^4} |x\rangle \otimes \hat{I}^{\otimes 4} + \sum_x^{2^4} (-1)^{\mathrm{Ham}(x)} |x\rangle \otimes \hat{Z}^{\otimes 4} \right) |\psi_4\rangle \\
&= \frac{1}{4\sqrt{2}} \left(\sum_x^{2^4} |x\rangle \otimes \hat{I}^{\otimes 4} + \sum_x^{2^4} (-1)^{\mathrm{Ham}(x)} |x\rangle \otimes \hat{Z}^{\otimes 4} \right) |\psi_4\rangle \\
&= \frac{1}{4\sqrt{2}} \left(\sum_x^{2^4} |x\rangle \otimes \left(\hat{I}^{\otimes 4} + (-1)^{\mathrm{Ham}(x)} \hat{Z}^{\otimes 4} \right) \right) |\psi_4\rangle \\
&= \frac{1}{4\sqrt{2}} \left(\sum_{\mathrm{Ham}(x)\ \mathrm{even}}^{2^4} |x\rangle \otimes \left(\hat{I}^{\otimes 4} + \hat{Z}^{\otimes 4} \right) + \sum_{\mathrm{Ham}(x)\ \mathrm{odd}}^{2^4} |x\rangle \otimes \left(\hat{I}^{\otimes 4} - \hat{Z}^{\otimes 4} \right) \right) |\psi_4\rangle ,
\end{aligned} \tag{2.4.13}$$

where we use x as a 4-binary string for the kets and $\mathrm{Ham}(x)$ is the hamming weight of bit string x.

Note that

$$\hat{I} + \hat{Z} = \hat{P}_0 \tag{2.4.14}$$

$$\hat{I}^{\otimes 2} + \hat{Z}^{\otimes 2} = \hat{P}_{00} + P_{11} \tag{2.4.15}$$

$$\cdots$$

$$\hat{I}^{\otimes n} + \hat{Z}^{\otimes n} = \sum_{\mathrm{Ham}(i)\ \mathrm{even}}^{2^n} \hat{P}_i \equiv P_{\mathrm{even}}, \tag{2.4.16}$$

and

$$\hat{I}^{\otimes n} - \hat{Z}^{\otimes n} = \sum_{\mathrm{Ham}(i)\ \mathrm{odd}}^{2^n} \hat{P}_i \equiv P_{\mathrm{odd}}, \tag{2.4.17}$$

where

$$P_i = |i\rangle\langle i| \tag{2.4.18}$$

is the projector of state i.

Eventually, 2.4.13 becomes

$$|\Psi_{stab}\rangle = \frac{1}{4\sqrt{2}} \left(\sum_{x\ \mathrm{even}}^{2^4} |x\rangle \otimes \hat{P}_{\mathrm{even}} + \sum_{\mathrm{odd}}^{2^4} |x\rangle \otimes \hat{P}_{\mathrm{odd}} \right) |\psi_4\rangle , \tag{2.4.19}$$

So, if we measure the auxiliary qubits to be in the x state, the Z parity [2] of the logical state among the 4 data qubits will be the same as the parity of x. Similarly, it is possible to find the X parity of 4 data qubits.

2.4.4. GHZ generation protocols

Now that we know that access to a 4-GHZ state enables stabilizer measurements among the 4 nodes, the question arises: How do we end up with this GHZ state when we can only entangle qubits in pairs? For this purpose, a plethora of protocols have been developed using various ways of intermediate distillation and different number of memory qubits [1, 4]. In our work, we shall restrict ourselves to only two simple GHZ generation protocols which we shall describe in this subsection: *Plain* [38] and *Modicum* [4].

[2] Since we are in the computational basis.

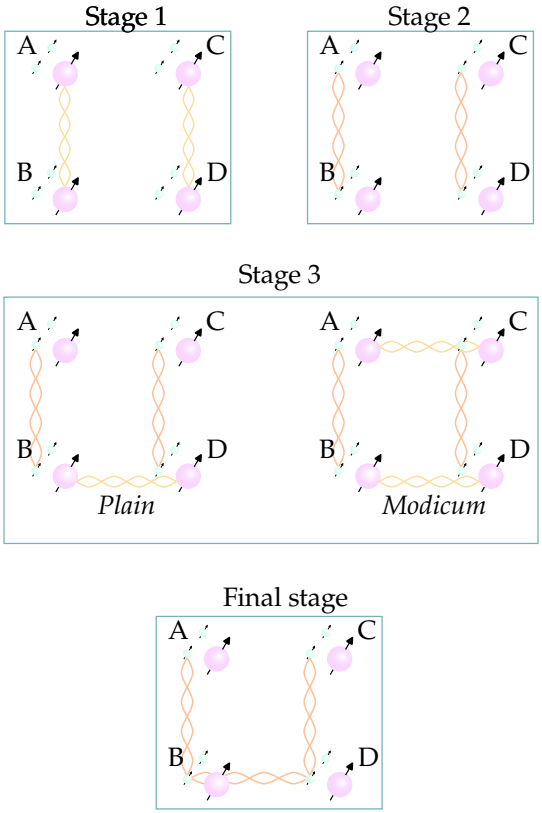

Figure 2.4: Sketch of the stages of the GHZ generation protocols *Plain* and *Modicum*.

To create a 4-GHZ state using two-qubit entangling gates, one could naively attempt 3 gates in succession. However, this is only a viable choice if the entangling gate is of high fidelity and succeeds with fairly high probability. The high fidelity constraint is important since a GHZ state of compromised fidelity will not allow for accurate stabilizer measurements. The high probability of success is vital as well, because the total probability of success will be p^3. If the probability of success is low enough, the expected time of successfully generating the GHZ state will be extremely high.

For these two reasons, distillation and fusion are employed, with the aid of quatum memory. Distillation is the process of consuming Bell pairs to create higher fidelity Bell pairs or increase the fidelity of multi-entangled states. The success probability issue is resolved by fusion, which is a probabilistic operation allowing us to merge two multi-entangled states of n_1 and n_2 qubits into a single multi-entangled state of $n_1 + n_2 - 1$ qubits. Thus, the creation of a high-fidelity GHZ state can be achievable even with access to entangling protocols with low probability of success and compromised fidelity.

Let us now describe the Plain protocol among 4 nodes A, B, C and D. The node pairs A-B and C-D attempt entanglement generation in parallel and as soon as they achieve it, they swap their entangled pairs into their quantum memory. At this stage, the pairs of nodes A-B and C-D have qubits that are entangled in their memory while their entanglement generation qubit has been freed up. Node A will now attempt entanglement generation with node C and as soon as this is accomplished, with two fusions we can merge the 3 Bell pairs into a 4-GHZ state.

Modicum differs from Plain only slightly. In the last generation attempt, instead of only attempting generation on the node pair A-C, we also attempt entanglement on the node pair B-D. The fusion procedure is the same, but in the end of it we have an extra Bell pair which we can use to purify the GHZ state further. Thus, by sacrificing a bit of the GHZ generation rate, we gain in fidelity.

We can see that these two protocols contain hardly any distillation, though. This means that the fidelity of the Bell pairs that we shall fuse together has to be quite high in order to achieve a high fidelity GHZ state. This may be done by purifying the Bell pairs multiple times before progressing to a next stage, or have high quality Bell pairs in advance.

3

Entangling Protocols for Distributed Architectures

Using the mechanisms described in section 2.4 allows us to attempt a fault-tolerant modular quantum computing approach. For this purpose, high fidelity GHZ states should be shared among stations of a few qubits that are connected among themselves [1]. This motivates us to look into entangling protocols that will be the foundation of these entangled states. For that reason we expand the protocol of Borregaard et al. (2015) [2] to accommodate distributed architectures.

3.1. Extra considerations

In this section we shall present additional considerations that are made in comparison to the original protocol.

3.1.1. Introducing fibers

To obtain distributed quantum computing architectures, we need some optical element to connect the computational nodes among themselves. This element will be optical fibers. The Hamiltonian of a fiber connected with two cavities that are connected to it is [39, 40]

$$H_{\text{fib}} = \omega_b \hat{b}^\dagger \hat{b} + \nu \left[\hat{b} \left(\hat{a}_1^\dagger + e^{i\varphi} \hat{a}_2^\dagger \right) + \text{ h.c.} \right], \tag{3.1.1}$$

where we have assumed that only one mode with frequency ω_b is relevant to our dynamics and $\hat{b}$ is the annihilation operator of the fiber field.

If we assume that the fiber length is l_b, the cavity length l_a and the cavity mirror transmission T, then the phase due to propagation in the fiber will be

$$\phi = \frac{2\pi\omega_b l_b}{c}, \tag{3.1.2}$$

and the coupling coefficient [41] is

$$\nu = \frac{c}{2}\sqrt{\frac{T}{l_b l_a}}, \tag{3.1.3}$$

where c the speed of light in the fiber.

The loss out of the fiber is described by the Lindblad operator

$$\hat{L}_b = \sqrt{\kappa_b}\hat{b}. \tag{3.1.4}$$

3.1.2. Allowing state $|0\rangle$ state excitations

In the original scheme [2], the qubit atom coupled to the cavity field only via an excitation of state $|1\rangle$. However, in our case we shall consider a more general setting where the $|0\rangle$ state will be allowed to be

excited to some excited state, and this transition will couple to the cavity mode that we are assuming to be present. This is motivated by the fact that this coupling is present in qubit implementations like SiV and SnV centers [21, 42].

Let's assume that state $|0\rangle$ couples to the cavity mode via the transition $|0\rangle \leftrightarrow |e_0\rangle$ where $|e_0\rangle$ is an excited state. Let this coupling be characterized by a coupling coefficient g_0 and a detuning Δ_{e0}. Also, let the excited state be susceptible to spontaneous emission into a dump state $|\tilde{o}_0\rangle$ with rate γ_0. The state $|1\rangle$ interactions shall remain the same, and we shall be adding the index 1 to the associated parameters and levels.

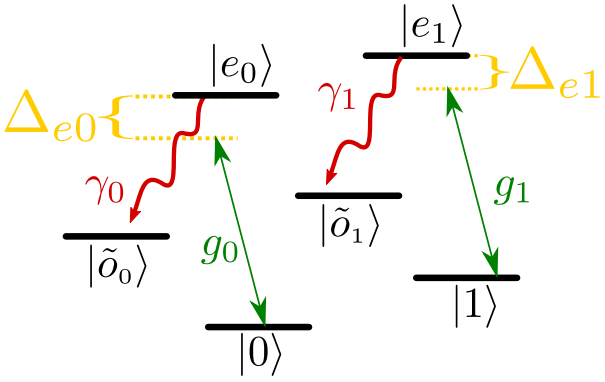

Figure 3.1: The qubit atom with state $|0\rangle$ coupled to an excited state.

Here we need to make a remark about the nature of states $|\tilde{o}_0\rangle$ and $|\tilde{o}_1\rangle$. Although they are considered isolated states, they could in fact coincide with $|0\rangle$ or $|1\rangle$, without any consequences for the dynamics. However, $|\tilde{o}_0\rangle$ and $|\tilde{o}_1\rangle$ should not coincide with each other. Thus:

$$\begin{aligned} |\tilde{o}_0\rangle = |0\rangle \,\&\, |\tilde{o}_1\rangle = |1\rangle \text{ is allowed,} \\ |\tilde{o}_1\rangle = |0\rangle \,\&\, |\tilde{o}_0\rangle = |1\rangle \text{ is allowed,} \\ |\tilde{o}_0\rangle = |\tilde{o}_1\rangle \text{ is not allowed.} \end{aligned} \tag{3.1.5}$$

The reason we exclude the case that the decayed states coincide with each other is because this would lead to a different total amplitude of the decayed states, thus leading to a different probability of success.

Last but not least, one may wonder why are we allowing only the qubit atoms to have this additional coupling. The auxiliary atom is still a qubit that we labelled as auxiliary, so it would make sense to include this coupling. To address this issue, let us consider the system state that would interact via this coupling:

$$|\Psi\rangle = \left|g\right\rangle \otimes \left|\psi^{\text{qubits}}_{\text{ground}}\right\rangle \otimes \left|1^{\text{aux}}_{\text{ph}}\right\rangle . \tag{3.1.6}$$

However, we are assumed that the evolution is adiabatic and that the auxiliary atom is initially in state $\left|g\right\rangle$. This means that for an excitation to be present in a cavity of the system, the auxiliary atom should be in state $\left|f\right\rangle$. As a result, this state is unattainable in the adiabatic regime, and we can neglect its coupling with the ground state subspace.

3.2. Dynamics of 0-x-0 in the interaction picture

In this section we shall present an extensive description of an entangling gate for distributed architectures. This gate is an expansion of the gate presented in Borregaard et al. (2015) [2]. The way it is different though is that we shall be assuming that each atom is in its own cavity, and the cavities are connected via optical fibers. We will assume that all cavities, qubit atoms and fibers are the same in terms of couplings and losses.

Due to this freedom of the geometry of the setup, it is good to use some notation to refer to each setup. Below we present the notation.

- x : Cavity containing auxiliary atom that is externally driven.
- 0 : Cavity containing qubit atom.

- - : Fiber connecting cavities. If it is the final element, it means that it connects the last cavity with the first one.

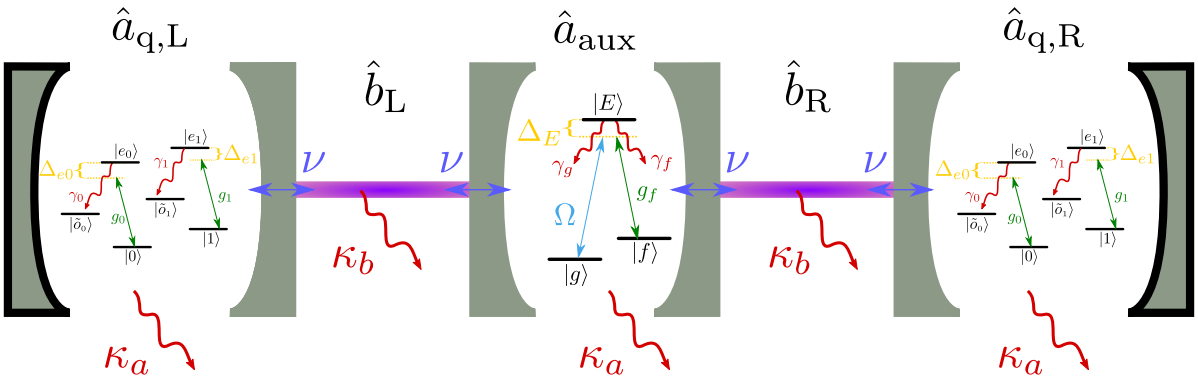

Figure 3.2: Sketch of the 0-x-0 scheme. The auxiliary atom is inside a two-sided cavity which is connected via optical fibers to two qubit atoms, each of which inside its own one-sided cavity.

As an example, we shall describe how the Hamiltonian is obtained in the interaction picture for a particular setup; specifically for 0-x-0.

The total bare Hamiltonian is

$$\hat{H}_{\mathrm{bare}} = \hat{H}_{\mathrm{aux}} + \hat{H}_{\mathrm{cav,aux}} + \sum_{k=\mathrm{L,\,R}} \hat{H}_{\mathrm{qubit},k} + \hat{H}_{\mathrm{cav},k} + \hat{H}_{\mathrm{fib},k}. \tag{3.2.1}$$

In the RWA, using the results of section 2.1 and neglecting the constant energy of the vacuum and of all other modes that do not interact with the atomic transitions, we obtain

$$\hat{H}_{\mathrm{cav},i} = \omega_{\mathrm{cav},i} \hat{a}_i^\dagger \hat{a}_i \tag{3.2.2}$$

$$\hat{H}_{\mathrm{aux}} = \omega_g |g\rangle\langle g| + \omega_f |f\rangle\langle f| + \omega_E |E\rangle\langle E| + \underbrace{\left(\Omega e^{i\omega_L t} |g\rangle\langle E| + \text{ h.c.}\right)}_{\text{laser int.}} + \underbrace{\left(g_f |E\rangle\langle f| \hat{a}_{\mathrm{aux}} + \text{h.c.}\right)}_{\text{cavity int.}}, \tag{3.2.3}$$

$$\hat{H}_{\mathrm{qubit}} = \omega_0 |0\rangle\langle 0| + \omega_1 |1\rangle\langle 1| + \omega_{\tilde{o}_0} |\tilde{o}_0\rangle\langle \tilde{o}_0| + \omega_{\tilde{o}_1} |\tilde{o}_1\rangle\langle \tilde{o}_1| + \underbrace{\left(g_0 |e_0\rangle\langle 0| \hat{a} + g_1 |e_1\rangle\langle 1| \hat{a} + \text{h.c.}\right)}_{\text{cavity int.}}, \tag{3.2.4}$$

$$\hat{H}_{\mathrm{fib}} = \omega_b \hat{b}^\dagger \hat{b} + \nu \left[\hat{b}\left(\hat{a}_{\mathrm{aux}}^\dagger + e^{i\varphi} \hat{a}^\dagger\right) + \text{ h.c.}\right]. \tag{3.2.5}$$

Note that in the above expressions for the fiber and the qubit, $k \in \{\mathrm{L, R}\}$ is omitted for brevity.

Now we shall select our rotating frame so that the Hamiltonian becomes time independent. The unitary operator of the rotating frame will be

$$\hat{U} = e^{it\hat{P}} \tag{3.2.6}$$

where $\hat{P}$ will be by choice a linear combination of all the projectors of the states appearing in the expression of $\hat{H}_{\mathrm{bare}}$, i.e.

$$\hat{P} = \sum_q c_q |q\rangle\langle q| \tag{3.2.7}$$

and thus,

$$\hat{U} = e^{it\hat{P}} = \sum_q e^{itc_q} |q\rangle\langle q| \tag{3.2.8}$$

The rotating frame as seen in 2.1.6 will be

$$\begin{aligned}\hat{H}_{\text{R.F.}} &= \hat{U}\hat{H}\hat{U}^\dagger + i\frac{d\hat{U}}{dt}\hat{U}^\dagger \\ &= \hat{U}\hat{H}\hat{U}^\dagger + i\left[\sum_q ic_q e^{itc_q}\left|q\right\rangle\!\left\langle q\right|\right]\left[\sum_{q'} e^{-itc_{q'}}\left|q'\right\rangle\!\left\langle q'\right|\right] \\ &= \hat{U}\hat{H}\hat{U}^\dagger - \sum_q c_q\left|q\right\rangle\!\left\langle q\right|. \end{aligned} \tag{3.2.9}$$

Also, for the field operators $\hat{q}$ we can define the transposition

$$\hat{q}^\dagger \longrightarrow e^{ic_q t}\hat{q}^\dagger \tag{3.2.10}$$

which is equivalent to taking the rotating frame of the Fock space of the photons as

$$\left|k\right\rangle_{\text{ph}} \longrightarrow e^{ikc_q t}\left|k\right\rangle_{\text{ph}}, \tag{3.2.11}$$

where k is the number of photons. This will lead to the transformation of the operator

$$\omega_q\hat{q}^\dagger\hat{q} \longrightarrow \left(\omega_q - kc_q\right)\hat{q}^\dagger\hat{q} \tag{3.2.12}$$

and since we are in the regime where we can have 0 or 1 photons, we can drop k.

Below we shall define c_q-s and their implications on the Hamiltonian:

$$c_g \longrightarrow \omega_g \Longrightarrow \begin{cases}\omega_g\left|g\right\rangle\!\left\langle g\right| & \longrightarrow 0 \\ \Omega e^{i\omega_L t}\left|g\right\rangle\!\left\langle E\right| & \longrightarrow \Omega e^{i\left(\omega_L+\omega_g\right)t}\left|g\right\rangle\!\left\langle E\right|\end{cases}, \tag{3.2.13}$$

$$c_E \longrightarrow -\left(\omega_L+\omega_g\right) \Longrightarrow \begin{cases}\omega_E\left|E\right\rangle\!\left\langle E\right| & \longrightarrow \Delta_E\left|E\right\rangle\!\left\langle E\right| \\ \Omega e^{i\left(\omega_L+\omega_g\right)t}\left|g\right\rangle\!\left\langle E\right| & \longrightarrow \Omega\left|g\right\rangle\!\left\langle E\right|\end{cases}, \tag{3.2.14}$$

where

$$\Delta_E = \omega_E - \omega_g - \omega_L \tag{3.2.15}$$

is the detuning associated with the transition $\left|g\right\rangle\!\left\langle E\right|$ due to the laser.

Note that even though we eliminated the time dependence from the term $\left|g\right\rangle\!\left\langle E\right|$, the vector $\left|E\right\rangle$ appears in other interactions and now will carry over time dependence. So, we need to keep specifying the rotating frame. For this reason, it is useful to organize everything in a table (see table 3.1).

We notice that no matter how many optical elements (cavities and fibers) we connect, their rotating frame should always be the same, namely:

$$\hat{q}^\dagger \longrightarrow e^{i\left(\omega_g+\omega_L-\omega_f\right)t}\hat{q}^\dagger \Longrightarrow \omega_q\hat{q}^\dagger\hat{q} \longrightarrow \left(\omega_q - \omega_g - \omega_L + \omega_f\right)\hat{q}^\dagger\hat{q}. \tag{3.2.16}$$

The Hamiltonian in the rotating frame will then become

$$\hat{H}^{\text{R.F.}} = \hat{H}^{\text{R.F.}}_{\text{aux}} + \hat{H}^{\text{R.F.}}_{\text{cav,aux}} + \sum_{k=\text{L, R}}\hat{H}^{\text{R.F.}}_{\text{qubit},k} + \hat{H}^{\text{R.F.}}_{\text{cav},k} + \hat{H}^{\text{R.F.}}_{\text{fib},k}, \tag{3.2.17}$$

where

$$\hat{H}^{\text{R.F.}}_{\text{cav},i} = \delta_{\text{cav},i}\hat{a}_i^\dagger\hat{a}_i, \tag{3.2.18}$$

$$\hat{H}^{\text{R.F.}}_{\text{aux}} = \Delta_E\left|E\right\rangle\!\left\langle E\right| + \underbrace{\left(\Omega\left|g\right\rangle\!\left\langle E\right| + \text{ h.c.}\right)}_{\text{laser int.}} + \underbrace{\left(g_f\left|E\right\rangle\!\left\langle f\right|\hat{a}_{\text{aux}} + \text{h.c.}\right)}_{\text{cavity int.}}, \tag{3.2.19}$$

$$\hat{H}^{\text{R.F.}}_{\text{qubit,k}} = \Delta_{e,k}\left|e_k\right\rangle\!\left\langle e_k\right| + \underbrace{\left(g\left|e_k\right\rangle\!\left\langle 1_k\right|\hat{a}_k + \text{h.c.}\right)}_{\text{cavity int.}}, \tag{3.2.20}$$

$$\hat{H}^{\text{R.F.}}_{\text{fib},k} = \delta_{b,k}\hat{b}_k^\dagger\hat{b}_k + \nu\left[\hat{b}_k\left(\hat{a}^\dagger_{\text{aux}} + e^{i\varphi}\hat{a}_k^\dagger\right) + \text{ h.c.}\right]. \tag{3.2.21}$$

$\|q\rangle$	c_q	Int.1	Prev	New	Int.2	Prev	New	Int.3	Prev	New
$\|g\rangle$	ω_g	$\|g\rangle\langle g\|$	ω_g	0	$\|g\rangle\langle E\|$	$\Omega e^{i\omega_L t}$	$\Omega e^{i(\omega_L+\omega_g)t}$	–	–	–
$\|E\rangle$	$\omega_g+\omega_L$	$\|E\rangle\langle E\|$	ω_E	Δ_E [a]	$\|g\rangle\langle E\|$	$\Omega e^{i(\omega_L+\omega_g)t}$	Ω	$\|E\rangle\langle f\|\hat{a}_{\text{aux}}$	g_f	$g_f e^{i(\omega_g+\omega_L)t}$
$\|f\rangle$	ω_f	$\|f\rangle\langle f\|$	ω_f	0	$\|E\rangle\langle f\|\hat{a}_{\text{aux}}$	$g_f e^{i(\omega_g+\omega_L)t}$	$g_f e^{i(\omega_g+\omega_L-\omega_f)t}$	–	–	–
$\hat{a}^\dagger_{\text{aux}}$	$\omega_g+\omega_L-\omega_f$	$\hat{a}_{\text{aux}}\hat{a}^\dagger_{\text{aux}}$	$\omega_{\text{cav,aux}}$	$\delta_{\text{cav aux}}$ [b]	$\|E\rangle\langle f\|\hat{a}_{\text{aux}}$	$g_f e^{i(\omega_g+\omega_L-\omega_f)t}$	g_f	$\hat{b}_{\text{L}}\hat{a}^\dagger_{\text{aux}}$	ν	$\nu e^{i(\omega_g+\omega_L-\omega_f)t}$
$\hat{b}^\dagger_{\text{L}}$	$\omega_g+\omega_L-\omega_f$	$\hat{b}^\dagger_{\text{L}}\hat{b}_{\text{L}}$	$\omega_{b,\text{L}}$	$\delta_{b,\text{L}}$ [c]	$\hat{b}_{\text{L}}\hat{a}^\dagger_{\text{aux}}$	$\nu e^{i(\omega_g+\omega_L-\omega_f)t}$	ν	$\hat{b}_{\text{L}}\hat{a}^\dagger_{\text{L}}$	$\nu e^{i\phi}$	$\nu e^{i[\phi-(\omega_g+\omega_L-\omega_f)t]}$
$\hat{a}^\dagger_{\text{L}}$	$\omega_g+\omega_L-\omega_f$	$\hat{a}^\dagger_{\text{L}}\hat{a}_{\text{L}}$	$\omega_{a,\text{L}}$	$\delta_{a,\text{L}}$ [d]	$\hat{b}_{\text{L}}\hat{a}^\dagger_{\text{L}}$	$\nu e^{i[\phi-(\omega_g+\omega_L-\omega_f)t]}$	$\nu e^{i\phi}$	$\|e_{\text{L}}\rangle\langle 1_{\text{L}}\|\hat{a}_L$	g	$g e^{-i(\omega_g+\omega_L-\omega_f)t}$
$\|1_{\text{L}}\rangle$	$\omega_{1,\text{L}}$	$\|1_{\text{L}}\rangle\langle 1_{\text{L}}\|$	$\omega_{1,\text{L}}$	0	$\|e_{1,\text{L}}\rangle\langle 1_{\text{L}}\|\hat{a}_L$	$g_1 e^{-i(\omega_g+\omega_L-\omega_f)t}$	$g_1 e^{-i(\omega_g+\omega_L-\omega_f+\omega_{1,\text{L}})t}$	–	–	–
$\|e_{1,\text{L}}\rangle$	$\omega_g+\omega_L-\omega_f+\omega_{1,\text{L}}$	$\|e_{1,\text{L}}\rangle\langle e_{1,\text{L}}\|$	$\omega_{e1,\text{L}}$	$\Delta_{e1,\text{L}}$ [e]	$\|e_{1,\text{L}}\rangle\langle 1_{\text{L}}\|\hat{a}_L$	$g_1 e^{-i(\omega_g+\omega_L-\omega_f+\omega_{1,\text{L}})t}$	g_1	–	–	–
$\|0_{\text{L}}\rangle$	$\omega_{0,\text{L}}$	$\|0_{\text{L}}\rangle\langle 0_{\text{L}}\|$	$\omega_{0,\text{L}}$	0	$\|e_{0,\text{L}}\rangle\langle 0_{\text{L}}\|\hat{a}_L$	$g_0 e^{-i(\omega_g+\omega_L-\omega_f)t}$	$g_0 e^{-i(\omega_g+\omega_L-\omega_f+\omega_{0,\text{L}})t}$	–	–	–
$\|e_{0,\text{L}}\rangle$	$\omega_g+\omega_L-\omega_f+\omega_{0,\text{L}}$	$\|e_{0,\text{L}}\rangle\langle e_{0,\text{L}}\|$	$\omega_{e0,\text{L}}$	$\Delta_{e0,\text{L}}$ [f]	$\|e_{0,\text{L}}\rangle\langle 0_{\text{L}}\|\hat{a}_L$	$g_0 e^{-i(\omega_g+\omega_L-\omega_f+\omega_{0,\text{L}})t}$	g_0	–	–	–
$\|\tilde{o}_{0,\text{L}}\rangle$	$\omega_{\tilde{o},\text{L}}$	$\|\tilde{o}_{0,\text{L}}\rangle\langle\tilde{o}_{0,\text{L}}\|$	$\omega_{\tilde{o}_0,\text{L}}$	0	–	–	–	–	–	–
$\|\tilde{o}_{1,\text{L}}\rangle$	$\omega_{\tilde{o},\text{L}}$	$\|\tilde{o}_{1,\text{L}}\rangle\langle\tilde{o}_{1,\text{L}}\|$	$\omega_{\tilde{o}_1,\text{L}}$	0	–	–	–	–	–	–

[a] $\Delta_E = \omega_E - \omega_g - \omega_L$
[b] $\delta_{\text{cav aux}} = \omega_{\text{cav,aux}} - (\omega_g + \omega_L - \omega_f)$
[c] $\delta_{b,\text{L}} = \omega_{b,\text{L}} - (\omega_g + \omega_L - \omega_f)$
[d] $\delta_{a,\text{L}} = \omega_{a,\text{L}} - (\omega_g + \omega_L - \omega_f)$
[e] $\Delta_{e1,\text{L}} = \omega_{e1,\text{L}} - \omega_g - \omega_L + \omega_f - \omega_{1,\text{L}}$
[f] $\Delta_{e0,\text{L}} = \omega_{e0,\text{L}} - \omega_g - \omega_L + \omega_f - \omega_{0,\text{L}}$

Table 3.1: Table summarizing rotating frame selection. The right part of the system will be the same as the left part due to symmetry.

3.3. Calculating effective dynamics using custom framework

The dynamics of the above Hamiltonian in the interaction picture can be calculated using the effective operator formalism from section 2.2. This intermezzo aims to present our methods for obtaining it, using our own custom computational framework which can be found here.

Assuming vacuum and $|g\rangle$ initialization, we can define the subspaces as follows:

- Ground state subspace spanned by:

$$|g\rangle \otimes \left\{ |00\rangle, |01\rangle, |10\rangle, |11\rangle \right\} \otimes |0_p\rangle \tag{3.3.1}$$

  of dimension $D_g = 4$.
- Excited state subspace spanned by:

$$\begin{gathered}
|f\rangle \otimes \left\{ |00\rangle, |01\rangle, |10\rangle, |11\rangle \right\} \otimes \left\{ |1_{a,\text{L}}\rangle, |1_{b,\text{L}}\rangle, |1_{a,\text{aux}}\rangle, |1_{b,\text{R}}\rangle, |1_{b,\text{R}}\rangle \right\}, \\
|E\rangle \otimes \left\{ |00\rangle, |01\rangle, |10\rangle, |11\rangle \right\} \otimes |0_p\rangle, \\
|f\rangle \otimes \left\{ |0e_0\rangle, |1e_0\rangle, |e_00\rangle, |e_01\rangle \right\} \otimes |0_p\rangle, \\
|f\rangle \otimes \left\{ |0e_1\rangle, |1e_1\rangle, |e_10\rangle, |e_11\rangle \right\} \otimes |0_p\rangle, \\
|f\rangle \otimes \left\{ |00\rangle, |01\rangle, |10\rangle, |11\rangle \right\} \otimes |0_p\rangle, \\
|f\rangle \otimes \left\{ |0\tilde{o}_0\rangle, |\tilde{o}_00\rangle, |1\tilde{o}_0\rangle, |\tilde{o}_01\rangle \right\} \otimes |0_p\rangle, \\
|f\rangle \otimes \left\{ |0\tilde{o}_1\rangle, |\tilde{o}_10\rangle, |1\tilde{o}_1\rangle, |\tilde{o}_11\rangle \right\} \otimes |0_p\rangle
\end{gathered} \tag{3.3.2}$$

  of dimension $D_e = 44$.

  Note that we shall be referring to the final 4 sets of states also as the *decayed* subspace as the excitation has been lost.

To make our calculations efficient, reliable and architecture independent, we developed a Python[43] framework to obtain analytically the effective operators from the rotating frame Hamiltonian. To this end, we utilize the sparse matrix representation for quantum systems of QuTip [44] package and the analytical expression superiority of Mathematica [45]. We link everything together with SageMath [46] which is a versatile mathematical package based on Python.

The way this is achieved is by defining every operator in the full tensor space, using QuTip's sparse matrix representation. This space contains all the states appearing in the Hamiltonian and Lindblad operators, but not above the first excitation of the fields, i.e. we treat them as two level systems. For example, in the case of `0-x-0` that would correspond to a space of dimension

$$\underbrace{6^2}_{\text{qub}} * \underbrace{2^3}_{\text{cav}} * \underbrace{2^2}_{\text{fib}} * \underbrace{3}_{\text{aux}} = 3456. \tag{3.3.3}$$

Then, the subspace is reduced to the tensor sum of ground state and first excited state subspace, all while keeping track of the labelling of the states. From that point on, Mathematica and SageMath take over.

The versatility of this framework comes from the fact that we can define any custom component like cavities, auxiliary atoms or qubit atoms, with any interactions we would like to incorporate. From these components, we define higher level elements like a cavity containing a specific atom or atoms. The whole system will then be comprised of a string of elements, connected via fibers, for example `0-x-0`.

As a correctness check to our calculations, we defined some setups of the original paper by Borregaard et al. (2015) [2] for 2 and 3 qubit atoms + 1 auxiliary atom in a cavity. The analytical results matched.

3.4. Squeezing the most out of the gate

To generate a Bell pair with the unitary, we shall follow the same procedure as described in section 2.3.2 for the CZ gate. However, as we have mentioned, dissipative dynamics will be present and will be affecting not only the probability of success but also the fidelity. In general, these effects can be partially mitigated by manipulating the gate time, along with single qubit rotations before and after the gate. The optimization of the gate time was also present in the original paper. In this section we shall be presenting this for the case of 2 qubits, but can be easily generalized.

To build up on the already existing way of implementing the gate, we shall consider these tweaks as a deviation from the standard circuit. We propose generalizing the initial state by applying a parametric $R_Y(\phi^i)$ gate on each qubit after the Hadamard gates. Similarly, for the output state, an additional parametric $R_Z(\phi^p)$ gate after the evolution. Lastly, we can in principle let the evolution run for a bit more or a bit less time, if it is deemed advantageous and let the new time duration be

$$\tilde{t}_g = r_{t_g} t_g, \tag{3.4.1}$$

where r_{t_g} some constant.

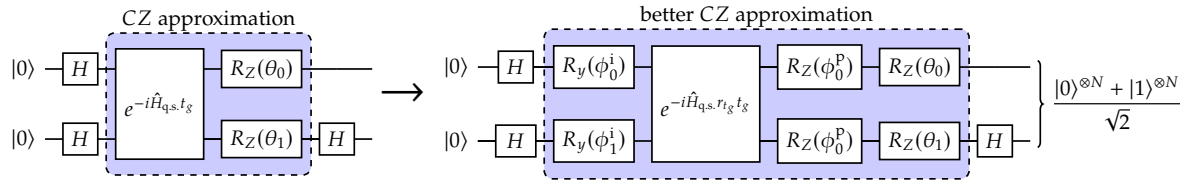

Figure 3.3: Circuit of the general circuit in comparison to the standard circuit. Note that θ rotations are not parametric rotations but rather fixed rotations.

The reasoning behind the selection of an R_Y gate after the Hadamard gate is that we are essentially initialize the system qubits to a state on the intersection of the Bloch sphere surface and the $x-z$ plane rather than to the special case of $|+\rangle$. Similarly, the post-gate corrections are better calibrated by adding the parametric R_Z gate. Note that while both of them improve the state fidelity, R_Y gates improve the concurrence of the state while R_z do not. That is because R_Z are local and act after the evolution.

This general treatment is better in terms of anticipating dissipative behavior of the system. Even if they are not eventually needed in some regime, the parameters of these corrections can be always set equal to zero.

3.5. Symmetry in the new setups

In the original paper [2] all the atoms were in a single cavity and the qubit atoms had the same detunings. This setup was completely symmetric and as a result the Hamiltonian, as can be seen in equation 2.3.16, was symmetric under any swap between the qubit excitations. The phase accumulation of each state of the ground state was thus dependent on only the number of qubits in state 1. However, this symmetry is now potentially broken by the architecture itself therefore allowing or forbidding some dynamics to happen.

Let us denote the Hamiltonian now on the qubit subspace as

$$\hat{H}_{\text{eff}} = \sum_{n=0}^{N} \Delta_n \hat{P}_n, \tag{3.5.1}$$

where n does not denote the number of excitations but rather a specific state and $\hat{P}_n$ is its projector.

For example, the scheme `x-0-0` is not symmetric since the qubit atoms are not connected the same way to the auxiliary atom. This means that the elements of the Hamiltonian will all be different in general. i.e.

$$\Delta_{00} \neq \Delta_{01} \neq \Delta_{10} \neq \Delta_{11}. \tag{3.5.2}$$

This still allows a CZ gate to be realized though but with single qubit rotations that are not equal to each other, similarly to the expression of 2.3.2. In contrast, the already described setup `0-x-0` will be symmetric like the scheme with 2 qubits + 1 auxiliary atoms in a single cavity. That is because all the elements are the same, thus there is no way to tell "left" from "right".

One very interesting setup is the cyclical `0-x-0-0-` setup. The last - denotes a fiber connecting the last cavity with the first one, as mentioned previously and seen in figure 3.4. If the first two cavity-atom systems are detuned and coupled similarly, then there will be no preference among the excitations of them. Consequently, this will lead to what we shall call *quasi-symmmetric* setups, since all but one of the diagonal elements of the Hamiltonian are symmetric with respect to swapping the qubits. The elements of the `0-x-0-0-` Hamiltonian will satisfy for example:

$$\Delta_{100} = \Delta_{010} \neq \Delta_{001} \qquad \& \qquad \Delta_{101} = \Delta_{011} \neq \Delta_{110}. \tag{3.5.3}$$

In the next section we shall show that under some conditions this can lead to the creation of a GHZ state with a single unitary.

3.6. Multi-entangling gates via quasi-symmetric setups

3.6.1. The CZZ gate

Let us investigate how in the context we are examining, a 3-partite entangling gate may be realized. In particular, we shall look into the three qubit gate CZZ, which can be decomposed into two Controlled-Z gates. We shall be following the same procedure as in section 2.3.2.

The unitary corresponding to the CZZ gate

$$\hat{U}_{CZZ} = \text{diag}(1, 1, 1, 1, 1, -1, -1, 1), \tag{3.6.1}$$

essentially giving a phase of -1 only to states $|101\rangle$ and $|110\rangle$.

To achieve this unitary, we select a quasi-symmetric setup such that:

$$\hat{U}(t) = \text{diag}(e^{iat}, e^{ibt}, e^{ibt}, e^{ict}, e^{idt}, e^{iet}, e^{iet}, e^{ift}). \tag{3.6.2}$$

Notice how the pairs states $|001\rangle$, $|010\rangle$ and $|101\rangle$, $|110\rangle$ have the same accumulation of phase as a result of their swap symmetry. The tensor product of the single qubit rotations will correspond to the unitary

$$\hat{R}_z(\boldsymbol{\theta}) = diag(1, e^{i\theta_1}, e^{i\theta_2}, e^{i(\theta_1+\theta_2)}, e^{i\theta_3}, e^{i(\theta_1+\theta_3)}, e^{i(\theta_2+\theta_3)}, e^{i(\theta_1+\theta_2+\theta_3)}). \tag{3.6.3}$$

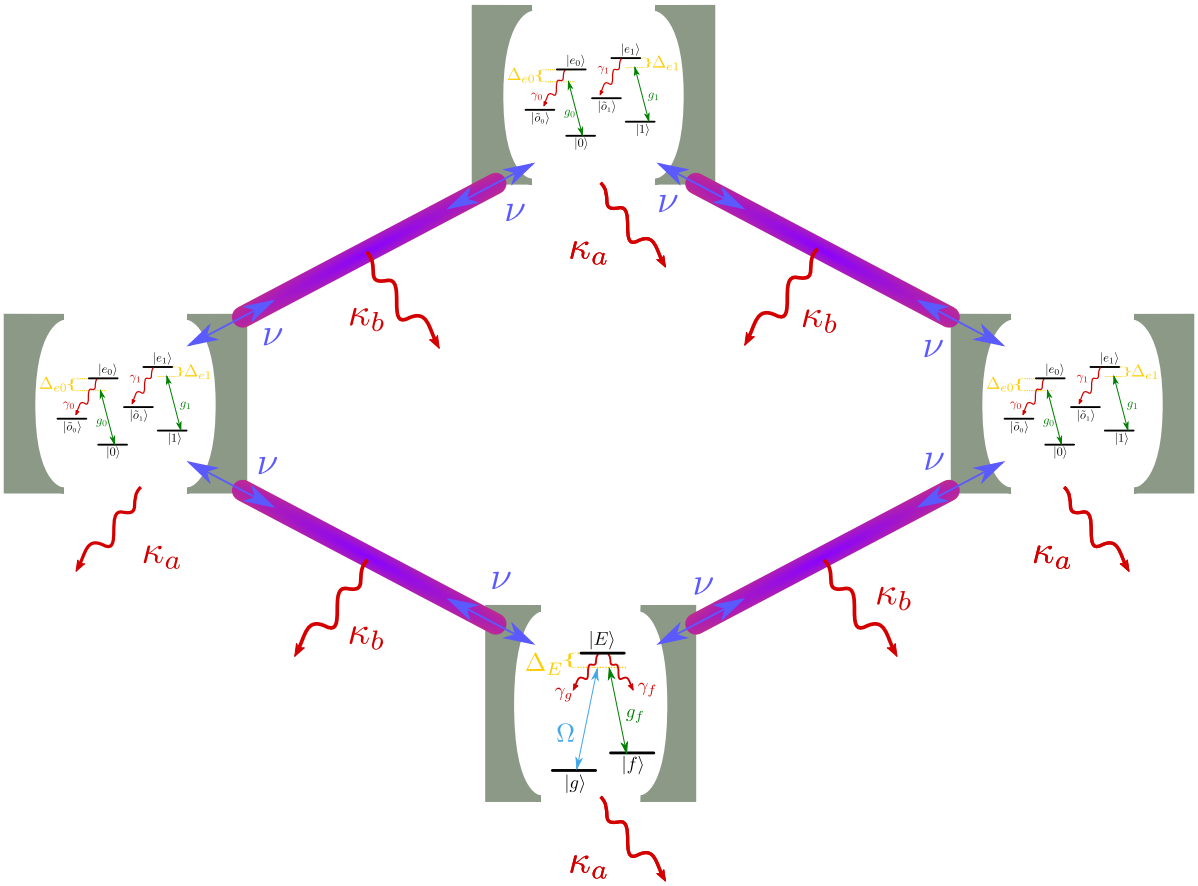

Figure 3.4: The 0-x-0-0- quasi-symmetric setup. The auxiliary atom is in the cavity in the bottom. Symmetry under qubit swapping applies to the two qubits on the left and right, but not for the one on top. This setup can implement a CZZ gate under some conditions.

Hence, to realize a CZZ gate, we need the conditions below to be satisfied:

$$\begin{aligned} \theta_1 &= \theta_2 \\ \theta_1 - (a-b)t &= 2n_1\pi \\ \theta_1 + \theta_2 - (a-c)t &= 2n_2\pi \\ \theta_3 - (a-d)t &= 2n_3\pi \\ \theta_1 + \theta_3 - (a-e)t &= (2n_4+1)\pi \\ \theta_1 + \theta_2 + \theta_3 - (a-f)t &= 2n_5\pi \end{aligned} \tag{3.6.4}$$

Selecting $n_1 = 0$ and $n_3 = 0$:

$$\begin{aligned} \theta_1 = \theta_2 &= (a-b)t \\ \theta_3 &= (a-d)t \\ t &= \frac{(2n_4+1)\pi}{a+e-b-d} \end{aligned} \tag{3.6.5}$$

Simultaneously, though we need the conditions

$$\begin{aligned} (a-2b+c)t &= 2n_2\pi \\ (2a-2b-d+f)t &= 2n_5\pi \end{aligned} \tag{3.6.6}$$

to be satisfied.

To realize this gate, one cannot simply enable the Hamiltonian interaction for a specified amount of time. The system has to also be tuned accordingly, such that conditions 3.6.6 are satisfied. This means

that although we gain in terms of generating the three-partite GHZ state with single entangling gate, the compromise due to those parameter restrictions may result in that gate being suboptimal.

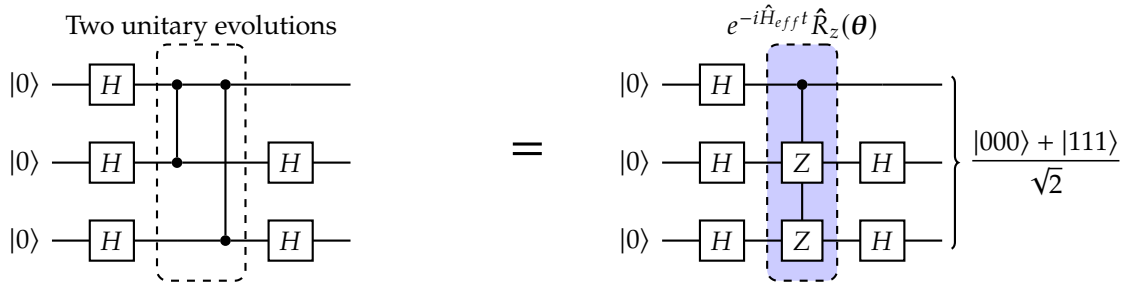

Figure 3.5: The 3-qubit entangling gate compared to a standard combination of CZ-gates. [1]

3.6.2. The CZ^N gate

In this section we shall attempt to generalize the multi-qubit entangling gate via quasi-symmetric[2] qubit Hamiltonian interactions. We shall show that given some conditions, a CZ^N gate can be implemented, which can be used to generate an $(N+1)$-partite GHZ state.

The CZ^N gate corresponds to the unitary:

$$CZ^N = \sum_{n=0}^{N} \Big(|0\rangle\langle 0| + (-1)^n |1\rangle\langle 1| \Big) \otimes \hat{P}_n, \tag{3.6.7}$$

where $\hat{P}_n$ is the sum of all the projectors with n qubits in state $|1\rangle$. This way, all states in which the first qubit is in state 1 and the rest of the N qubits have an odd $Z^{\otimes 2N}$ parity, will attain a phase -1.

Let us consider now the quasi-symmetric Hamiltonian. We shall be calling control qubit the qubit that is excluded from the swap symmetry, causing the quasi-symmetry of the system. The rest of the qubits shall be called target qubits. The quasi-symmetric Hamiltonian will be

$$\hat{H}_{\text{q.s.}} = \sum_{n=0}^{N} \Big(a_{0,n} |0\rangle\langle 0| + a_{1,n} |1\rangle\langle 1| \Big) \otimes \hat{P}_n, \tag{3.6.8}$$

where $a_{i,n}$ is the energy of the system when the control qubit is in state $i \in [0,1]$ and n of the target qubits are in state 1.

The unitary evolution generated by this in time t_g will be

$$\hat{U}_{\text{q.s.}} = \sum_{n=0}^{N} \Big(e^{-ia_{0,n}t_g} |0\rangle\langle 0| + e^{-ia_{1,n}t_g} |1\rangle\langle 1| \Big) \otimes \hat{P}_n \tag{3.6.9}$$

The total unitary need not be exactly the CZ^N gate but rather the same up to single qubit rotations. Let us consider that we operate with $\hat{R}_Z$ rotations on the qubits. To preserve the quasi-symmetry of the unitary, all rotations should be the same, except for the one acting on the control qubit. Let these rotations be θ_1 and θ_1 respectively. Since,

$$\hat{R}_Z(\theta) = |0\rangle\langle 0| + e^{i\theta} |1\rangle\langle 1|, \tag{3.6.10}$$

then,

$$\hat{R}_Z(\theta_0, \theta_1) = \sum_{n=0}^{N} \Big(|0\rangle\langle 0| + e^{i\theta_0} |1\rangle\langle 1| \Big) \otimes e^{in\theta_1} \hat{P}_n. \tag{3.6.11}$$

[1] The quantum circuits were generated using Quantikz [47].

[2] See section 3.5 for the definition.

As a result, to generate a CZ^N gate in a single step, the condition

$$\hat{U}_{\text{q.s.}}\hat{R}_Z(\theta_0,\theta_1) = CZ^N \tag{3.6.12}$$

should be satisfied, where

$$\begin{aligned}\hat{U}_{\text{q.s.}}\hat{R}_Z(\theta_0,\theta_1) &= \sum_{n=0}^{N}\left(e^{-ia_{0,n}t_g}\,|0\rangle\langle 0| + e^{i\theta_0}e^{-ia_{1,n}t_g}\,|1\rangle\langle 1|\right)\otimes e^{in\theta_1}\hat{P}_n \\ &= \sum_{n=0}^{N}\left(e^{i(n\theta_1-a_{0,n}t_g)}\,|0\rangle\langle 0| + e^{i(\theta_0+n\theta_1-a_{1,n}t_g)}\,|1\rangle\langle 1|\right)\otimes \hat{P}_n.\end{aligned} \tag{3.6.13}$$

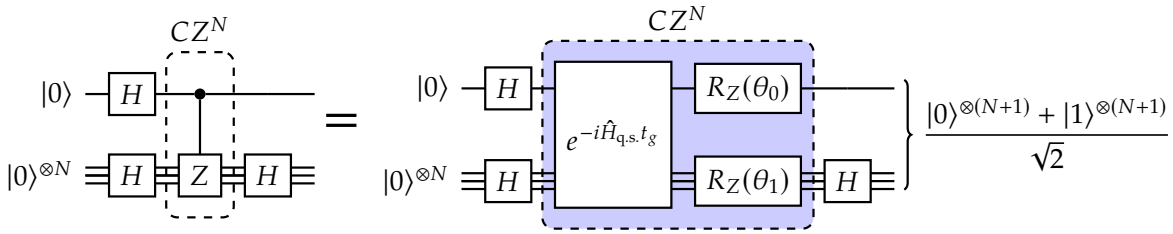

Figure 3.6: The N-qubit entangling gate compared to a standard combination of CZ-gates.

Now let us reflect on this condition while comparing with the expression of CZ^N from equation 3.6.7. For the gate to be generated, $2N+2$ equations should be simultaneously satisfied. However, we can freely select the time t_g and the two rotations θ_0 and θ_1, such that 3 equations of those are always satisfied. Also, the global phase can be ignored and as a result one more equation may be ignored. Eventually, the CZ^N gate will be able to be generated as long as $2N-2$ extra equations are satisfied. For $N=2$, we fall into the category of three-partite GHZ states using a CZZ gate, and we need $2\cdot 2-2=2$ extra conditions to be satisfied, as shown in the previous subsection.

Of course, chances are that we will not stumble across a Hamiltonian which has this property of satisfying these extra $2N-2$ relations. It is rather necessary that we select the experimental parameters of the underlying Hamiltonian mechanism such that these conditions are satisfied. Also, this might mean that the gate although possible, may be suboptimal in comparison to the combined action of N CZ gates. That is because in the trivial case that $N=1$, no extra conditions need to be satisfied. Thus, the experimental parameters may be selected to optimize the gate performance, since the plausibility of the gate is a given. Regardless, one should be on the lookout for these Hamiltonian interactions since they have the potential of generating the GHZ state, thus enabling non-local stabilizer measurements.

Some final remarks need to be made about these conditions, that facilitate the plausibility of the gate. First, the Hamiltonian and rotation expressions correspond to phases that should either be 1 or -1 and

$$1 = e^{2k\pi i} \qquad \& \qquad -1 = e^{(2k+1)\pi i} \qquad \text{for } k \text{ integer.} \tag{3.6.14}$$

This means that one can select for each expression one more free integer parameter k. Moreover, in realistic scenarios the fidelity is compromised due to losses, regardless of the plausibility of the gate. Thus, the condition don't need to be satisfied exactly but rather up to some degree.

Note that the original intracavity protocol is described by such a quasi-symmetric Hamiltonian if one equalizes all but one of the qubit detunings.

4

Analytical and Numerical Results

4.1. Analytical results for 0-x-0

In this section we shall present some analytical results as an example of the capabilities of the software that we developed. In addition, we shall use the analytical results to select the parameter regime in which the gate is scalable.

4.1.1. Emerging quantities

The effective Hamiltonian and Lindblad operators can be written as a function of the bare operator parameters. However, notation and physical intuition of the results is largely enhanced by introducing parameters that combine these low level parameters into higher level parameters.

We shall set the transition $|1\rangle \leftrightarrow |e_1\rangle$ as reference, to reduce the amount of indices in the expressions. Namely,

$$\gamma \coloneqq \gamma_1 \qquad g \coloneqq g_1, \tag{4.1.1}$$

so that we can write every spontaneous decay rate and cavity coupling in terms of that via the ratios

$$R_i \coloneqq \frac{g_i^2}{g^2} \tag{4.1.2}$$

$$r_i \coloneqq \frac{\gamma_i}{\gamma}. \tag{4.1.3}$$

Two very frequently occurring quantities that shall arise are the *atom-cavity cooperativity*

$$C \coloneqq \frac{g^2}{\kappa_c \gamma} \tag{4.1.4}$$

and the *fiber-cavity cooperativity*

$$c \coloneqq \frac{v^2}{\kappa_c \kappa_b}, \tag{4.1.5}$$

both of which quantify the coupling of the cavity field with the fiber with regard to the losses from the Lindblad operators.

Also, from the non-Hermitian Hamiltonian of the quantum-jump formalism, the detunings shall always appear in the effective operators as

$$\begin{aligned} \tilde{\Delta}_{e1} &= \Delta_{e1}/\gamma - i/2, \\ \tilde{\Delta}_{e0} &= \Delta_e/\gamma - i r_0/2, \\ \tilde{\Delta}_E &= \Delta_E/\gamma - i(r_f + r_g)/2 \\ \tilde{\delta}_c &= \delta_c/\gamma - i\kappa_c/(2\gamma), \\ \tilde{\delta}_b &= \delta_b/\gamma - i\kappa_b/(2\gamma). \end{aligned} \tag{4.1.6}$$

Based on the previous expressions, we can define an even higher level parameter, describing the transition couplings that takes into account the detuning and the cooperativity. We shall be calling *effective cooperativity* associated with a transition that is detuned by Δ_{ei} (or Δ_E for $i = E$) the quantity

$$\tilde{C}_i \coloneqq \frac{CR_j}{\tilde{\Delta}_i}, \tag{4.1.7}$$

where R_j will be the quantity of the transition as defined in equation 4.1.2. In particular,

$$\tilde{C}_0 = \frac{CR_0}{\tilde{\Delta}_{e0}}, \qquad \tilde{C}_1 = \frac{C}{\tilde{\Delta}_{e1}}, \qquad \tilde{C}_E = \frac{CR_f}{\tilde{\Delta}_E}. \tag{4.1.8}$$

Some other expressions that arise without a trivial physical interpretation are the expressions

$$c_a \coloneqq c + \frac{1}{2^a} \tag{4.1.9}$$

and the polynomials

$$\begin{aligned} P_1(c) &\coloneqq 16\,c^2 + 12\,c + 1, \\ P_2(c) &\coloneqq 48\,c^2 + 16\,c + 1. \end{aligned} \tag{4.1.10}$$

With all of this notation, we can define the final notations that will allow for brevity in the analytical expressions. Namely, the expressions

$$\begin{aligned} A_i = A_{\overline{xy}} &\coloneqq 2\,P_1(c)\left(\tilde{C}_x + \tilde{C}_y\right) + iP_2(c) - i\tilde{C}_x\tilde{C}_y c_3, \\ B_i = B_{\overline{xy}} &\coloneqq 2\left(\tilde{C}_x + \tilde{C}_y\right)c_2 - \tilde{C}_x\tilde{C}_y + 4c_2^2, \end{aligned} \tag{4.1.11}$$

where $\overline{xy}$ is the 2-bit representation of the integer $i \in \{0, 1, 2, 3\}$.

With all of this relatively complicated but incredibly compact notation, we can proceed to present the analytical results obtained by the framework we developed.

4.1.2. Effective Hamiltonian and Lindblad operators

The effective Hamiltonian is diagonal and of the form

$$\hat{H}^{\text{eff}}_{0\text{-}\mathbf{x}\text{-}0} = \sum_{x=0}^{3} \Delta_x \left|x\right\rangle\!\left\langle x\right|, \tag{4.1.12}$$

where

$$\Delta_x = -\frac{\Omega^2}{\gamma}\,\text{Re}\left\{\frac{A_x}{8\,B_x\tilde{C}_E + A_x}\,\frac{1}{\tilde{\Delta}_E}\right\}, \tag{4.1.13}$$

assuming that the cavities and the fibers are on resonance

$$\delta_c = \delta_b = 0. \tag{4.1.14}$$

As one may notice, the Hamiltonian is symmetric under the swap of qubits. Namely, one could "switch the labels" between "left" and "right", and the time evolution of the system would still be the same. This can be seen by the fact that

$$\Delta_{\overline{01}} = \Delta_{\overline{10}} \tag{4.1.15}$$

The losses of the 0-x-0 setup are described in total by 11 Lindblad operators. However, only the ones in the central auxiliary atom-cavity system will preserve this left-right symmetry. This will lead to the analytical notation becoming more and more obtuse as this symmetry is lost. Luckily, the auxiliary atom losses can be easily written as

$$\hat{L}_{\text{eff},\gamma_g} = \frac{\Omega}{\tilde{\Delta}_E\sqrt{\gamma}}\sqrt{r_g}\sum_{x=0}^{3}\frac{A_x}{8\,B_x\tilde{C}_E + A_x}\left|g\right\rangle\!\left\langle E\right| \otimes \hat{P}_x\,, \tag{4.1.16}$$

$$\hat{L}_{\text{eff},\gamma_f} = \frac{\Omega}{\tilde{\Delta}_E\sqrt{\gamma}}\sqrt{r_f}\sum_{x=0}^{3}\frac{A_x}{8\,B_x\tilde{C}_E + A_x}\,|f\rangle\langle E|\otimes\hat{P}_x \tag{4.1.17}$$

Unfortunately, this compact notation that we have devised, fails from this point and on to encapsulate the dynamics elegantly. As an example, we shall present the Lindblad operator corresponding to the loss out of the auxiliary cavity.

For this we shall define the polynomials:

$$\begin{aligned} P_3(c) &\coloneqq 8c^2 + 12c + 1 \\ P_4(c) &\coloneqq 24c^2 + 12c + 1 \end{aligned} \tag{4.1.18}$$

and the quantities

$$\begin{aligned} K_{0,\overline{xy}} &\coloneqq 4\tilde{C}_{s,\overline{xy}}P_3c_2^2 + \tilde{C}_{p,\overline{xy}}\tilde{C}_{s,\overline{xy}}P_4 + 8i\tilde{C}_{p,\overline{xy}}^2c_3 - i\left(\tilde{C}_{s,\overline{xy}}^2P_1 - 2\tilde{C}_{p,\overline{xy}}P_1 - P_2\right)c_2, \\ K_{1,\overline{xy}} &\coloneqq -16i\,\tilde{C}_{s,\overline{xy}}c_2^3 + 16\,c_2^4 + 4\,\tilde{C}_{p,\overline{xy}}\tilde{C}_{s,\overline{xy}}c_2 - 4\left(\tilde{C}_{s,\overline{xy}}^2 - 2\,\tilde{C}_{p,\overline{xy}}\right)c_2^2 + \tilde{C}_{p,\overline{xy}}^2, \end{aligned} \tag{4.1.19}$$

where

$$\begin{aligned} \tilde{C}_{p,\overline{xy}} &\coloneqq \tilde{C}_0\,\tilde{C}_1, \\ \tilde{C}_{s,\overline{xy}} &\coloneqq \tilde{C}_0 + \tilde{C}_1. \end{aligned} \tag{4.1.20}$$

This leads to an auxiliary cavity loss described by the Lindblad operator

$$\hat{L}_{\text{eff},\kappa_{aux}} = 32\,\frac{\sqrt{\tilde{C}_E}\Omega}{\sqrt{\tilde{\Delta}_E}\sqrt{\gamma}}\sum_{x=0}^{3}\frac{2K_1\tilde{C}_E + K_0}{\left(2\,B_x\tilde{C}_E + A_x\right)^2}\,\hat{P}_x\otimes|f\rangle\langle g|\,. \tag{4.1.21}$$

As a courtesy to the reader, we shall not continue with this the lengthy notation. One way to simplify the notation and maybe obtain presentable results, would be to assume that some cooperativites are the same. For the purposes of this report, we shall not go into that though.

It is important to note that by introducing the cooperativity parameters, we eliminated the dependency on $\nu, g, \kappa_b, \kappa_c$. This will only be the case though, when the fibers and the cavities are on resonance. If they are not, the quantities $\tilde{\delta}_c$ and $\tilde{\delta}_b$ will appear in the effective operators. These quantities are dependent on the values of κ_c and κ_b and therefore their value cannot be ignored.

4.1.3. Scaling of the scheme

It is important that the scheme scales well. This means that one would expect that by improving experimental setups, one would expect the gate to perform better and better. The Hamiltonian parameters that describe the efficiency of the experimental setup are the two cooperativites C and c. Let's take a step back and notice the implications of our analytical results in the high cooperativity limit.

We shall assume that

$$\begin{aligned} \tilde{\Delta}_E \sim C^n \Leftrightarrow \Delta_E \sim \gamma C^n, \\ \Omega \sim \gamma C^m. \\ c \approx C \end{aligned} \tag{4.1.22}$$

For $C \gg 1$ the gate time as derived in section 2.3.2 can be found that it scales as

$$t_g \approx C^{n-2m}\,\frac{1}{\gamma} \tag{4.1.23}$$

The losses per state s can be estimated by the expression

$$(\text{Loss})_s \approx \sum_i |l_{i,s,\text{eff}}|^2\,t_g \tag{4.1.24}$$

where $l_{i,s,\text{eff}}$ is every element of the Lindblad operators acting on state s.

Looking into the full expressions of the losses, we find out that the only way to suppress both field and spontaneous emission losses, is to select

$$\Delta_E \sim \sqrt{C} \Leftrightarrow n = 1/2, \tag{4.1.25}$$

which leads to the losses scaling as

$$(\text{Loss}) \sim \frac{1}{\sqrt{C}}. \tag{4.1.26}$$

However, from 2.3, in order for the driving to be adiabatic the condition

$$\frac{\Omega g}{\Delta_E} \ll \kappa_c \tag{4.1.27}$$

needs to be satisfied and thus to keep a low adiabatic error without compromising the gate time, we select

$$\Omega = \epsilon\gamma\sqrt{C}, \tag{4.1.28}$$

where ϵ is appropriately small.

Eventually, the scalings for the losses and the gate time will be

$$\begin{aligned} t_g &\sim \frac{1}{\sqrt{C}}, \\ (\text{Loss}) &\sim \frac{1}{\sqrt{C}}. \end{aligned} \tag{4.1.29}$$

Note that the same selection was done in the original paper [2].

4.1.4. Cavity-fiber cooperativity to coupling efficiency

One of the quantities that we introduced previously was the cavity-fiber cooperativity

$$c \coloneqq \frac{\nu^2}{\kappa_c \kappa_b}. \tag{4.1.30}$$

This quantity, although very useful for our analytical results, it fails to convey the hardware restrictions it implies. The experimental values for the coupling of the cavity to the fiber are given as a probability of a photon being transmitted into the fiber instead of being lost, also known as *coupling efficiency* and symbolized with η [48]. For this reason, we need to find the conversion between those two.

The cavity-fiber interaction Hamiltonian reads

$$\hat{H}_{\text{int}} = \nu\left(e^{i\phi}\hat{b}\hat{c}^\dagger + e^{-i\phi}\hat{b}^\dagger\hat{c}\right) \tag{4.1.31}$$

and the loss operators are

$$\begin{aligned} \hat{L}_c &= \sqrt{\kappa_c}\hat{c}, \\ \hat{L}_b &= \sqrt{\kappa_b}\hat{b}. \end{aligned} \tag{4.1.32}$$

The effective non-hermitian Hamiltonian will be:

$$\hat{H}_{\text{NH}} = \hat{H}_{\text{int}} - \frac{i}{2}\sum_{j=c,b}\hat{L}_j^\dagger\hat{L}_j. \tag{4.1.33}$$

The Heisenberg equation of motion for an operator $\hat{a}$ is

$$\dot{\hat{a}} = -i[\hat{a}, \hat{H}] \tag{4.1.34}$$

which leads to the coupled differential equations

$$\begin{cases} \dot{\hat{c}} = i\nu\hat{b} - \frac{\kappa_c}{2}\hat{c} \\ \dot{\hat{b}} = i\nu\hat{c} - \frac{\kappa_b}{2}\hat{b} \end{cases}. \tag{4.1.35}$$

In the regime where

$$\nu \ll \kappa_b \Rightarrow c \ll \frac{\kappa_b}{\kappa_c}, \tag{4.1.36}$$

we can adiabatically eliminate the excited states and make the simplification

$$\begin{aligned} \cancelto{0}{\dot{\hat{b}}} &= i\nu\hat{c} - \frac{\kappa_b}{2}\hat{b} \\ \Rightarrow \hat{b} &= \frac{2i\nu}{\kappa_b}\hat{c} \end{aligned} \tag{4.1.37}$$

Substituting back to the cavity mode differential equation we get

$$\dot{\hat{c}} = -\underbrace{\left(\frac{2\nu^2}{\kappa_b} + \frac{\kappa_c}{2}\right)}_{\Gamma}\hat{c}, \tag{4.1.38}$$

which has as solution the time dependent amplitude

$$\hat{c} = \hat{c}(t=0)e^{-\Gamma t}. \tag{4.1.39}$$

This leads to an intensity of:

$$I = <\hat{c}^\dagger\hat{c}> \sim e^{-2\Gamma t} \tag{4.1.40}$$

As a result, total rate out of the cavity will be 2Γ which is due to both transmission into the fiber and loss of the photon. The rate that goes into the fiber is:

$$\Gamma_b = 2\Gamma - \kappa_c = \frac{4\nu^2}{\kappa_b} \tag{4.1.41}$$

Thus, the coupling efficiency will be

$$\eta = \frac{\Gamma_b}{2\Gamma} = \frac{4\nu^2/\kappa_b}{\frac{4\nu^2}{\kappa_b} + \kappa_c} \tag{4.1.42}$$

$$\boxed{\eta = \frac{4c}{4c+1},} \tag{4.1.43}$$

or equivalently

$$\boxed{c = \frac{\eta}{4-4\eta}.} \tag{4.1.44}$$

4.2. Numerical Methods

Before we go into the numerical results of this report, it is important that we discuss our methods of obtaining them. We shall employ two main methods to obtain the output density matrix of the evolution: *superoperator* simulations and *analytical* approximations.

4.2.1. Superoperator Simulations

As we have mentioned earlier in 2.2, the evolution of a density matrix in a dissipative environment is the solution of the Lindblad master equation

$$\dot{\rho} = -i\left[\hat{H}_{\text{eff}}, \rho\right] + \sum_k \hat{L}^k_{\text{eff}}\rho\left(\hat{L}^k_{\text{eff}}\right)^\dagger - \frac{1}{2}\left[\left(\hat{L}^k_{\text{eff}}\right)^\dagger\hat{L}^k_{\text{eff}}\rho + \rho\left(\hat{L}^k_{\text{eff}}\right)^\dagger\hat{L}^k_{\text{eff}}\right]. \tag{4.2.1}$$

Since the dynamics are not time dependent, the density matrix output can be calculated as

$$\rho(t) = e^{i\mathscr{L}t}\,\rho_0 \tag{4.2.2}$$

where ρ_0 the initial density matrix and $\mathscr{L}$ is the superoperator[49] describing the dissipative evolution.

To act with the superoperator on the density matrix we need to vectorize the density matrix

$$\rho \rightarrow |\rho\rangle\rangle. \tag{4.2.3}$$

The summands of the superoperator are terms $\hat{A}$ multiplying the density matrix ρ left-wise($\mathcal{L}$), right-wise($\mathcal{R}$) or both. These summands can be calculated as

$$\begin{aligned} \hat{A}\rho &\longrightarrow (A \otimes I)|\rho\rangle\rangle = \mathcal{L}(A)[\rho] \\ \rho\hat{A} &\longrightarrow (I \otimes A)|\rho\rangle\rangle = \mathcal{R}(A)[\rho] \end{aligned} \tag{4.2.4}$$

where $|\rho\rangle\rangle$ is the vectorized density matrix.

For the dimensions of the density matrix, one would naively assume that we can just use the ground state subspace to describe it. However, since all but one Lindblad operators make the system go to a decayed state, we need to include these states in the description. As mentioned in 3.1.2, we cannot merge all of those dump states into one single dump state, as this would create interactions between them, which our model does not contain.

Thus, if we are calculating the dynamics of `0-x-0`, the density matrix should be 16×16, due to the ground state being 4-dimensional and the decayed subspace being 12-dimensional. The superoperator will then be a 256×256 matrix since $256 = 16^2$.

These simulations allow us to fully encapsulate the dynamics of the gate. Although these are quite fast, [1] when optimization is needed, this approach fails to give results quickly enough. To this end, we shall use the analytical approximation method, presented in the next subsection, which is much quicker.

4.2.2. Analytical Approximations

Let's assume that the effect of undetectable errors is negligible. The loss of fidelity will then originate solely from the uneven losses of each state, as described in 2.3.2. Given that we already have the analytical expressions generated for every operator, we can use them to obtain analytical expressions for the probability of success and the fidelity, thus making the calculations much faster.

However, we have to not be deceived by the appeal of this approach, and it is important that we are cautious for this method to be faster. The reason behind this is that the fidelity's analytical expression can be extremely lengthy if it is obtained in terms of the bare Hamiltonian and Lindblad elements.[2] This would lead to the analytical expressions being even slower than the superoperator simulations.

Instead, we employ a *matryoshka* approach.[3] Since each quantity contains lower level quantities, it is optimal to start the numerical substitution from the lowest level and express higher level quantities as a function of the lower level quantities, shortening the expressions as much as possible. In descending order of levels, the quantities are

$$F \longleftarrow P_s \longleftarrow t_g \longleftarrow \left\{\hat{H}^{\text{eff}}, \hat{L}^{\text{eff}}\right\} \longleftarrow \left\{\hat{H}^{\text{bare}}, \hat{L}^{\text{bare}}\right\} \tag{4.2.5}$$

4.3. Parameter Selection

A final clarification that needs to be made has to do with the parameter setting that we shall be using. Let it be known that we separate the parameter in three categories:

- *General parameters* that shall be fixed throughout the rest of the report and ensure adiabaticity and partially define the hardware.
- *Hardware Constraints* that correspond to the hardware components that are the weakest link and compromise the performance.
- *Tunable parameters* or *tuning* will be the set of parameters that we shall consider that we are free to select such that we achieve optimal performance.

In this section we shall present the selected parameters for the numerical simulations. It is important to note that these do not constitute restrictions but rather hardware inspired values that comply with

[1] For the `0-x-0` simulations it took $\sim$ 0.3sec for a single simulation on a gaming laptop.
[2] Compactifying these elements into expressions dependent on cooperativites as we did in 4.1.2 may not be always possible.
[3] Matryoshka, also known as Russian doll, is a set of nested wooden dolls, which resembles the structure of the problem.

the restrictions. We shall be using them to produce numerical results and showcase the possibilities of this scheme. As mentioned earlier, one could even revisit the assumption that every cavity, fiber and atom are of the same nature with the same parameters.

4.3.1. General Parameters

First and foremost, the spontaneous decay γ of the excited state $|e1\rangle$ will be set at 30MHz. This value however is not realistic, and it stems from an overlook that we only identified at the final stages of the project. The actual realistic value would be 2π 30 MHz for Tin-Vacancy spins in diamond [21, 50, 51].

The timescale of our simulations is therefore set as $1/\gamma$. This means that our miscalculation will lead us to be pessimistic about the gate since the actual evolution time would in fact be $1/(2\pi)$ of the numerical values we present in realistic scenarios. In terms of code, we can set $\gamma = 1$. Now, almost everything needs to be given as a function of γ.

Assuming that the transition $|0\rangle \leftrightarrow |e0\rangle$ is of the same nature as $|1\rangle \leftrightarrow |e1\rangle$, we can set

$$\gamma_0 = \gamma, \tag{4.3.1}$$

and since the auxiliary atom is a qubit atom that is externally driven, the spontaneous emission rate out of state $|E\rangle$ will be

$$\gamma_f + \gamma_g = \gamma. \tag{4.3.2}$$

We will allow suppression of the undetectable decay $|E\rangle \rightarrow \big|g\big\rangle$ to the point that

$$\begin{aligned} \gamma_g &= 0.05\gamma, \\ \gamma_f &= 0.95\gamma. \end{aligned} \tag{4.3.3}$$

This suppression is made by means of external magnetic field to orient the spin electron appropriately [21].

The decay rates κ_c and κ_b do not need to be set because the effective expressions are not dependent on them. This comes as a result of setting them on resonance, i.e.:

$$\delta_c = \delta_b = 0 \tag{4.3.4}$$

However, to avoid the need for algebraic simplifications we shall be setting arbitrarily

$$\begin{aligned} \kappa_c &= 100\, C\, \gamma, \\ \kappa_b &= 100\, c\, \kappa_c, \end{aligned} \tag{4.3.5}$$

which will not affect the dynamics, but the adiabaticity will be preserved in case we assume off-resonant cavity or fiber modes, according to 2.3.14. Simultaneously, the mapping from the coupling efficiency to the cavity fiber cooperativity shall still be valid. Talking about adiabaticity, we shall be setting

$$\Omega = \frac{1}{8}\gamma\sqrt{C}, \tag{4.3.6}$$

similarly to the original paper [2]. [4]

We shall not be assuming that any qubit atom, fiber or cavity is different from the others, unless stated otherwise. The couplings of transitions to the cavities shall all be the same

$$g_f = g_0 = g_1 = g, \tag{4.3.7}$$

and we shall be assuming that we are in the short fiber limit, such that from equation 3.1.2 we get

$$\phi = 0. \tag{4.3.8}$$

[4] Note that our definition of Ω differs by a factor of two in comparison to the original paper.

4.3.2. Hardware Constraints

In this category there will be two parameters: the cavity-fiber cooperativity c and the maximum splitting $\Delta_{\max}$.

In subsection 4.1.4, we presented the equivalency of cavity-fiber cooperativity and coupling efficiency. For SiV centers in diamonds, experimental coupling efficiency of $\eta = 93\%$ has been achieved experimentally, which is equivalent to a mere $c \approx 3.3$ [42]. For the atom-cavity cooperativity though, the experimental values are much more encouraging. Values of $C \approx 100$ have been achieved experimentally in SiV centers [42], and for SnV centers cavity-SnV center coupling efficiencies of 95% [52], which is equivalent to $C = 4.5$ in our model.

We can see that there is a disparity among the two cooperativities with the cavity-fiber cooperativity lagging behind the cavity-atom cooperativity. Simultaneously, we discussed how the two cooperativites should be of the same order for the gate to scale well. Motivated by these facts, we will be assuming that the atom-cavity cooperativity is a tunable parameter, rather than a hardware constraint, as we might have to compromise its maximum attainable value in order for the gate to perform well. This could be experimentally challenging, since this might entail very precise fabrication, but in principle, it might be possible by means of reducing the coupling strength or increasing the loss rates out of the cavity-atom system. Hence, the cavity-fiber coupling efficiency or equivalently, the cooperativity c is the only hardware constraint of the two.

As discussed in subsection section 3.1.2, the inclusion of the $|0\rangle$ state coupling was inspired by implementations like SnV and SiV centers. The detunings that one would naively select arbitrarily though shall also have constraints, though. We shall assume that there is some maximum optical separation of the states, which will act as an upper bound. This maximum detuning split will be

$$\Delta_{\max} \geq |\Delta_{e0} - \Delta_{e1}| \,. \tag{4.3.9}$$

This $\Delta_{\max}$, again depends on the implementation. SnV centers in cavities have demonstrated values of $\approx 70\gamma$ [21], but we shall be modest in our selection to accommodate more potential implementations. We shall restrict ourselves to a maximum value of 20γ.

4.3.3. Tunable Parameters

The final set of parameters is where the optimization will come into play.

Firstly, all the detunings can be selected in a way that is optimal, respecting always the previous assumptions that we made. This selection may be possible again by appropriately tweaking the cavity resonance frequency, the external classical field and the energy levels of the states by modifying the external magnetic field that induces them [42]. The auxiliary atom detuning as we mentioned earlier will be selected to scale as

$$\Delta_E = \beta\gamma\sqrt{C} \tag{4.3.10}$$

and given the adiabaticity condition we conclude that we can select β so long as

$$\beta \gg 1/80 = 0.0125. \tag{4.3.11}$$

We shall respect this condition by only allowing

$$\beta \geq 1. \tag{4.3.12}$$

The detunings of the atoms Δ_{e0}, Δ_{e1} may also be selected freely so long as

$$\Delta_{\max} \geq |\Delta_{e0} - \Delta_{e1}| \tag{4.3.13}$$

is not violated. The qubit detuning of $\Delta_{e,s}$ associated with the transition $|s\rangle \leftrightarrow |e,s\rangle$ affects the effective phase accumulation of ground state $|s\rangle$. Thus, if we were to select $\Delta_{e0} = \Delta_{e1}$, the evolution would generate just a global phase on the initial state, since all 4 ground states would be accumulating the same phase over the evolution. As a result, in general it is important that we make use of all the splitting, i.e.

$$\Delta_{\max} = |\Delta_{e0} - \Delta_{e1}| \,, \tag{4.3.14}$$

and in particular to seek the optimum point when the relative difference of Δ_{e0}, Δ_{e1} is not compromised too much. Remembering also that the nature of states $|0\rangle$ and $|1\rangle$ was assumed to be the same, we

General		Tuning		Hardware	
Param	Value	Param	Value	Param	Value
γ_0	γ	Δ_E	$[\gamma\sqrt{C}, +\infty]$	η	~ 0.9
γ_g	0.05γ	Δ_e	$[0, \Delta_{\max}]$	$\Delta_{\max}$	$\sim 10\gamma$
γ_f	0.95γ	C	$\sim c$	–	–
δ_c, δ_b	0	r_{t_g}	$(0, +\infty]$	–	–
κ_c	$100\,C\,\gamma$	$\phi_{0,1}^{\mathrm{i,p}}$	$[-\frac{\pi}{2}, \frac{\pi}{2}]$	–	–
κ_b	$100\,c\,\kappa_c$	–	–	–	–
g_0, g_f	g	–	–	–	–
Ω	$\frac{1}{8}\gamma\sqrt{C}$	–	–	–	–
ϕ	0	–	–	–	–
Δ_{e0}	$\Delta_{\max} - \Delta_e$	–	–	–	–

Table 4.1: All the parameters that are used in the simulation. Note that γ,g and Δ_e are quantities associated with the transition $|0\rangle \leftrightarrow |1\rangle$.

understand that it does not matter which of the two is larger, we can conclude to selecting

$$\begin{aligned} 0 \leq \Delta_e \leq \Delta_{\max}, \\ \Delta_{e0} = \Delta_{\max} - \Delta_e, \end{aligned} \tag{4.3.15}$$

consequently categorizing Δ_{e0} as a general parameter.

Moreover, as foreshadowed in section 3.4, it should be experimentally straightforward to tweak the time of the evolution or the single qubit gates prior and after the evolution. Thus, the angles ϕ and the constant r_{t_g} that we defined in the aforementioned section shall be allowed to vary to our advantage.

Finally, as mentioned earlier, we shall allow the cavity fiber cooperativity C to be tuned and its optimum will be sought in the vicinity of c.

4.4. Verification of scalings

Before we go into optimizing the gate, it is important that we verify that our selection of parameters was correct in terms of scaling.

In figure 4.1 we plot the performance of the gate against cooperativity without optimizing for the original protocol, using the library *Matplotlib* [53] and superoperator simulations. The detuning of the auxiliary atom is scaling simply

$$\Delta_E = \sqrt{C}, \tag{4.4.1}$$

and the detuning of the excitation of state $|1\rangle$ is in both cases

$$\Delta_e = \Delta_{e1} = 0. \tag{4.4.2}$$

For `0-x-0`, the cavity-fiber and the cavity-atom cooperativities match

$$c = C, \tag{4.4.3}$$

and the detuning of the $|0\rangle$ state coupling is selected to be

$$\Delta_{e0} = 10^3\, C, \tag{4.4.4}$$

such that at any given time the effective cooperativity of this transition is much smaller

$$\tilde{C}_0 \ll \tilde{C}_1. \tag{4.4.5}$$

This effectively means that we eliminate the $|0\rangle$ state coupling to the cavity, similarly to the original version of the atomic states. This leads to the rapidest accumulation of phase difference among states $|0\rangle$ and $|1\rangle$, which is optimal for the gate. Any non mentioned parameter is set as defined in section 4.3.

In the resulting logarithmic plots, we can clearly see that in all cases, the performance error metrics scale as predicted, namely with the inverse square root of the cooperativity

$$t_g, 1 - P_s, 1 - F \sim \frac{1}{\sqrt{C}}. \tag{4.4.6}$$

This can be identified by the tendency of all curves when reaching the high cooperativity regime.

By comparison of the two protocols, the presence of extra losses of `0-x-0` can also be identified. Firstly, the probability of failure is consistently higher than the intracavity protocol, which is purely due to the surplus of detectable losses. This surplus is due to the additional optical elements, i.e. two extra cavities and two extra fibers.

The fidelity is slightly lower which is because the undetectable losses are identical, while the equality of cooperativities allows for similar dissipative behavior for the fibers and the cavities. As the cooperativity increases, the difference between dissipative losses due to detectable losses is becoming less and less relevant.

The gate time, has the same behavior, despite the fact that visually it does not seem so. This is a consequence of our choice to normalize its value to the maximum value it attains in the sweep which facilitates the simultaneous visualization of the performance.

At this point, one could be deceived and believe that the extra considerations we made in comparison to the initial protocol, do not matter all that much in terms of losses. However, the values of the cooperativity here are futuristic, especially for the case of the fiber-cavity cooperativity. More importantly, here we essentially eliminated the hardware constraint of limited optical separation between the two transitions of the qubit atom. If instead we assume a heuristically inspired scaling

$$\Delta_{\max} = \sqrt{C} \tag{4.4.7}$$

of the maximum splitting, we shall obtain the results of Figure 4.2.

Immediately, the effect of this constraint is apparent. In the high cooperativity limit, the infidelity increased by one order of magnitude, while the probability of success is underwhelming, given the futuristic aspect of the values. For lower cooperativities, the gate time skyrocketed 2 orders of magnitude while the probability of failure is closer to the value 1 than the float-point precision of Python, which is $\approx 10^{-15}$. The point that this takes place can be seen in the fidelity curve as a non-physical jump.

4.5. Optimization

Now that we have established that we can select the parameters in such a way that the gate scales well with the cooperativity, it is time to optimize it for specific hardware constraints.

4.5.1. Hyperparameters

The aforementioned hyperparameters of the GHZ creation are parameters that we shall fix throughout the optimization, and they are inspired by state-of-the-art NV centers [54]. We present them in table 4.2. The nodes are remotely entangled using electronic spins and the nuclear spin acts as a quantum memory.

Given all of these, we shall define a variant of the gate time, which we shall call *effective gate time*

$$t_g^{\text{eff}} := t_{\text{evolution}} + t_{\text{single qubit gates}} + t_{\text{measure and reset}}, \tag{4.5.1}$$

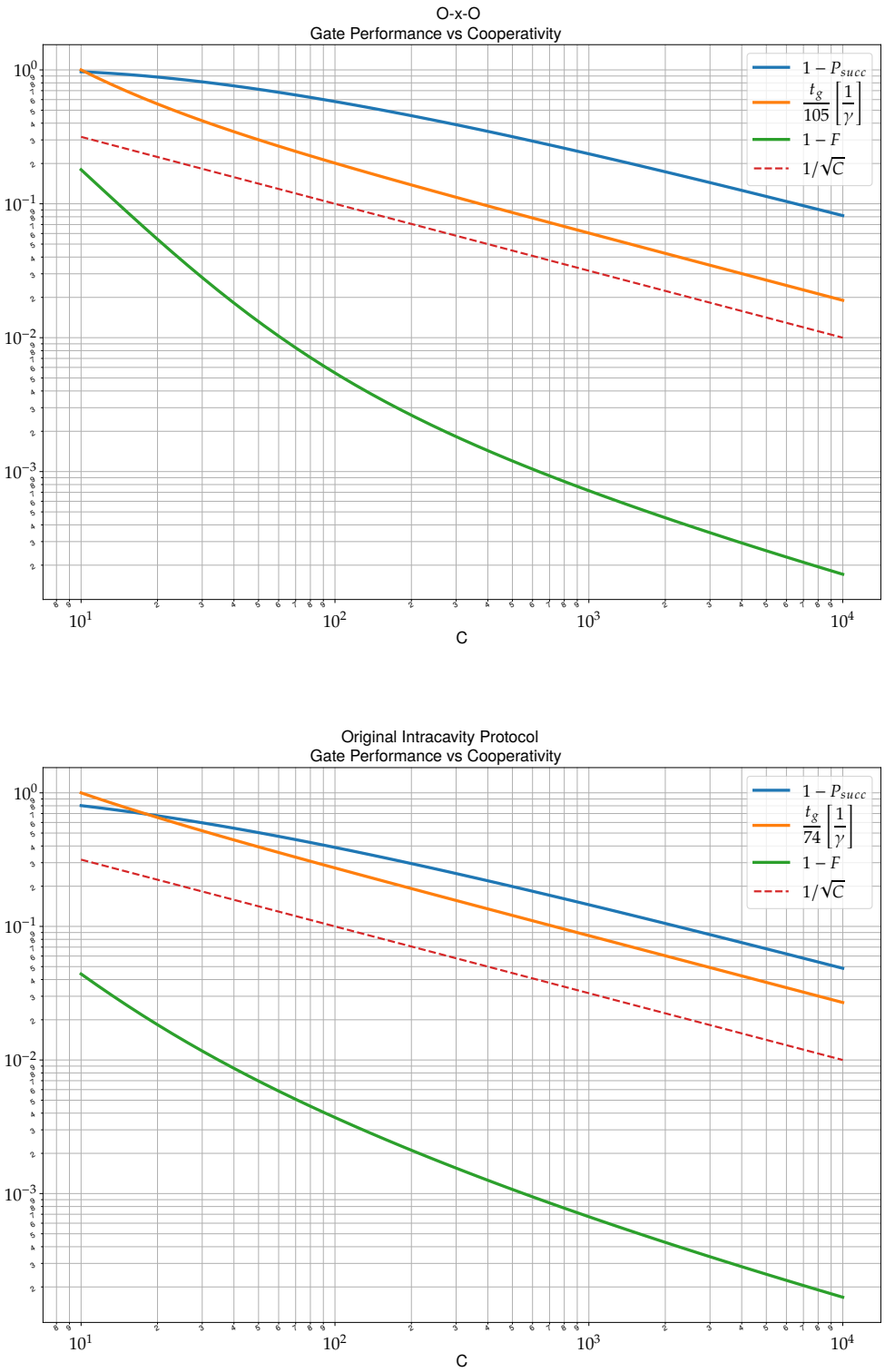

Figure 4.1: Performance of 0-x-0 and of the original protocol proposed in [2] as a function of cooperativity. Note that the gate time is scaled with the maximum value of the sweep.
Parameters
For both : $\Delta_E = \sqrt{C}$, $\Delta_e = \Delta_{e1} = 0$
For 0-x-0 : $c = C$, $\Delta_{e0} = 10^3\, C$

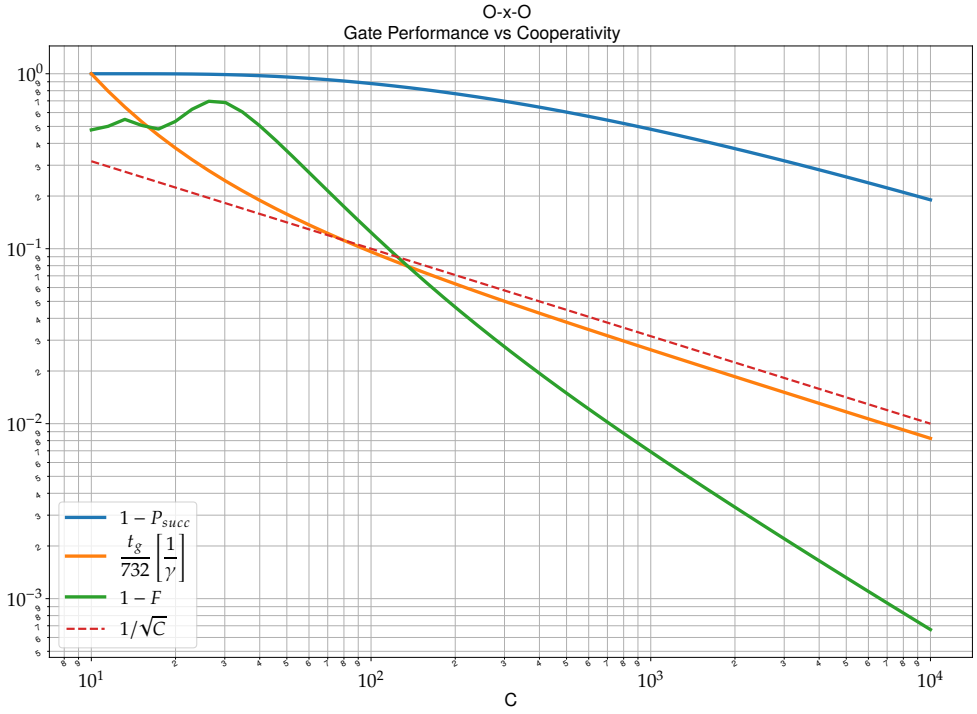

Figure 4.2: Performance of `0-x-0` under constrained maximum detuning split. The abnormality of fidelity is non-physical and is a result of the probability of failure surpassing the float-point precision of Python ($\approx 10^{-15}$).
Parameters: $\Delta_E = \sqrt{C}$, $c = C$, $\Delta_{e1} = 0$ $\Delta_{e0} = \sqrt{C}$

Operation	t_{measure}	$t^{\text{e}}_{\text{single qubit}}$	$t^{\text{n}}_{\text{single qubit}}$	$t_{\text{CX(n,e)}}$	$t_{\text{SWAP(n,e)}}$
Duration	$4\mu s$	$0.1\mu s$	$0.5ms$	$0.5ms$	$1.5ms$

Table 4.2: Time for various operations that correspond to state-of-the-art NV-architectures [54].

where

$$\begin{aligned} t_{\text{evolution}} &= \tilde{t}_g = r_{t_g}\, t_g, \\ t_{\text{single qubit gates}} &= 2\, t^{\text{e}}_{\text{H}}, \\ t_{\text{measure and reset}} &= 2\, t_{\text{measure}}. \end{aligned} \tag{4.5.2}$$

The last quantity is the time to see if the gate was successful and in case it was not, reset the qubit atoms by measuring them, as a means of initialization.

4.5.2. Cost function

An optimization algorithm aims to minimize some cost function by varying some parameters. It is pretty straightforward that the parameters that shall be varying will be the tuning, while the rest of parameters of section 4.3 will act as model hyperparameters. The cost function should translate the performance of the gate into a single real number that the smaller it is, the better the performance ranks. Let us define the performance as a tuple of the fidelity, the probability of success and the gate time in units of 1γ:

$$\text{Performance} := (F, P_s, t_g) \tag{4.5.3}$$

We define our cost function heuristically as

$$\lambda_c \coloneqq \begin{cases} F_{\text{cap}} - F & \text{if } F < F_{\text{cap}} \\ -\dfrac{1}{t_{0.99}} & \text{if } F \geq F_{\text{cap}} \end{cases}, \tag{4.5.4}$$

where F_{cap} is some fidelity cap and $t_{0.99}$ the 99% temporal confidence interval.

The x temporal confidence interval t_x shall be defined as the time needed to succeed in the creation of a GHZ state with probability x, i.e.

$$t_x \;=\; t_g^{\text{eff}}\, \mathcal{F}_x(P_s) + t_{\text{swap}}, \tag{4.5.5}$$

where $\mathcal{F}$ the cumulative distribution of the random variable describing the GHZ generation. We see that this metric encapsulates the rate with which the GHZ states can be generated, taking into consideration both the time and the probability of success. We select this metric rather than the average time in order to capture the full distribution behavior. Note that this will also include the time needed to swap the entanglement into the memory t_{swap}. This choice is motivated by the fact that the swapping time will be the bottleneck if the gate creates the Bell pairs very rapidly.

To understand how the cost function shall behave let us assume that we set a fidelity cap $F_{\text{cap}} = 95\%$ and the initial tuning leads randomly to a performance of e.g. $(F = 0.7, P_s = 0.01, t_g = 56)$. Since the fidelity is below the fidelity cap, the optimizer shall for now neglect the values of P_s and t_g, trying to increase the fidelity since the cost function is a decreasing function of F. Once the fidelity cap is reached, the optimizer shall start attempting to decrease the 99% temporal confidence interval as now the function is an increasing function of $t_{0.99}$. However, this has to be done in such a way that the fidelity does not drop below the fidelity cap.

This allows us to set some exact fidelity which we need to achieve. As a result, it is ensured that the fidelity of the output state is not too low which would mean that we need to change our GHZ creation protocol. A lower fidelity would mean that intermediate steps of distillation are needed to achieve a high fidelity GHZ state.

Simultaneously though, it makes sure that the fidelity is not higher than we actually need. This might sound counter-intuitive but in realistic scenarios we shall be limited by other weak links of the chain. For example, if the readout error is 95%, achieving a 99% GHZ fidelity might be unnecessary. Not only that, but also we sacrificed optimization of the parameters that could have gone into improving the temporal interval of confidence instead.

4.5.3. Optimization Results

Now that we have established our methods of simulations, we shall proceed to present our findings.

We optimized the gate for $\eta \in [0.9, 0.95, 0.99]$ in combination with $\Delta_{\text{max}} \in [3, 5, 10, 20]$ with a fidelity cap $F_{\text{cap}} = 99\%$. The minimization of the cost function was sought while the tunable parameters were in the bounds presented in table 4.3 using the analytical approximation method, and the results of the optimization can be found in figure 4.3.

Parameter	Minimum	Maximum
Δ_E	$\gamma\sqrt{C}$	$20\gamma\sqrt{C}$
Δ_e	0	Δ_{max}
r_{t_g}	0.7	1.1
C	$0.1\,c$	$10\,c$
$\phi_{0,1}^{\text{i,p}}$	$-\pi/2$	$\pi/2$

Table 4.3: Tuning optimization bounds.

The minimization algorithm was selected to be *differential evolution*, implemented by *SciPy* [55, 56]. This is a global minimization algorithm which is stochastic and not gradient based. Thus, we do not need

to guess the initial state but only the bounds to be investigated. SciPy's implementation polishes the optimization result by running the gradient descent algorithm *L-BFGS-B* on the output of the differential evolution [57, 58]. As a means of precaution against local minima, we ran the routine multiple times. The final plotting was done using *seaborn* [59].

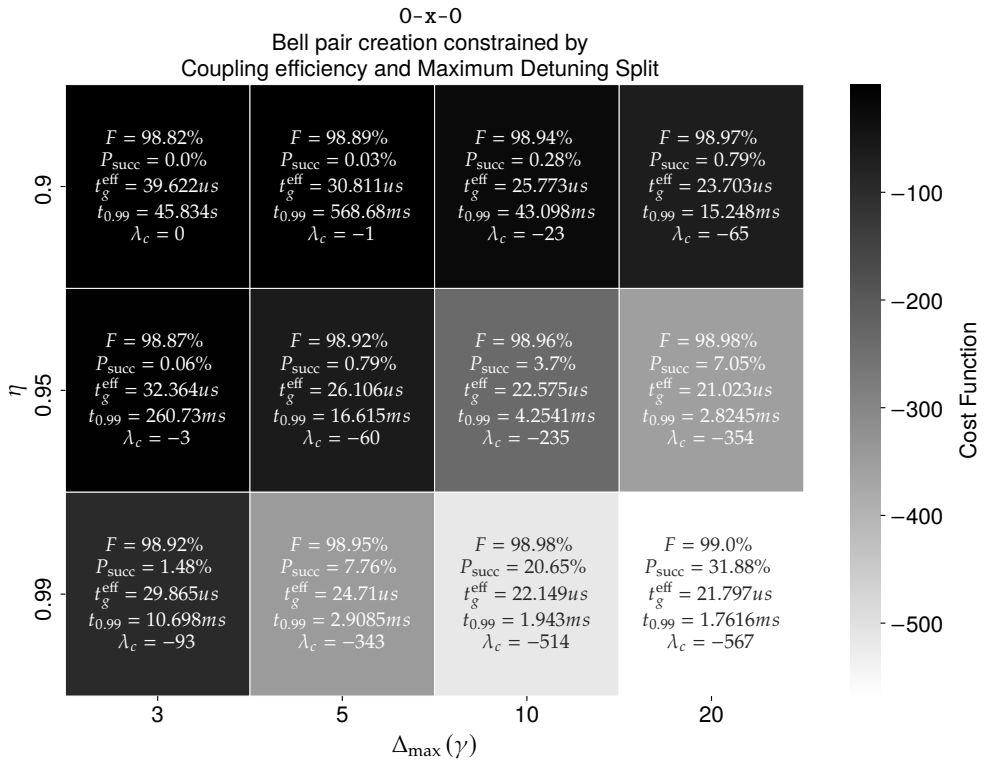

Figure 4.3: Optimized performance of `0-x-0` for different combination of hardware constraints. Optimization was done with analytical approximations with a fidelity cap $F_{cap} = 99\%$. The presented fidelity is from the superoperator simulation when using the tuning found via the optimization.

The first thing we notice, is that the performance of the gate is an increasing function of η and $\Delta_{\max}$, as was expected from the investigations of section 4.4. Moreover, the better the performance, the less is the effect of the undetectable loss γ_g. Remember that the optimization was done with a fidelity cap of 99% and the analytical approximation did not take into consideration the undetectable loss. Thus, the deviance from 99% is due to the inclusion of γ_g.

Something else to notice is that the effective gate time seems to be capping at around $20\mu s$. This is because from the definition of t_g^{eff} in equation 4.5.1, it contains some constants that correspond to the time needed to initialize, measure and reset which act as a bottleneck. These sum to $9\mu s$. As a result, it is not deemed advantageous to make the evolution time smaller than this order of magnitude, since $9\mu s$ is the minimum value that the effective gate time can achieve.

Similarly, the 99% temporal interval of confidence seems to be converging to a value around $1.5ms$. That is because the bottleneck in that case is the swapping of the entanglement into the memory qubits, which takes $1.5ms$.

At this point it is important to remember that our initial value for γ was off by a factor of approximately 6 for realistic scenarios. This means that for the same t_g^{eff} we could have achieved higher probabilities of success and thus lower temporal intervals of confidence.

4.6. Comparison with emission based protocol

Having obtained this optimized set of entangling gates for various hardware constraints, we shall proceed to compare them with another entangling protocol. Since our motivation was achieving fault tolerance in distributed architectures, we shall test our gate against a more standard emission based

scheme on their efficiency when creating 4-GHZ states.

We shall not delve into the emission based protocols, since it is outside the scope of this thesis. The main idea though is that the electronic spins of the two nodes are each in a superposition of two metastable states, one of which is able to emit a photon when excited by an external source. The two nodes are simultaneously excited and emit photons towards a common beam splitter. The trajectory of the photons are perpendicular to each other while forming an angle of $\pi/4$ with the beam splitter, such that the reflected mode of each source coincides spatially with the transmitted mode of the other. If we measure on the outgoing modes only one photon, then the two photon sources shall become entangled. That is because the photon could have originated from either source.

Our GHZ creation simulations will output for every entangling protocol the average time it took to generate a 4-GHZ state and the average output fidelity. To put our protocol into perspective, we shall use the protocol Modicum to perform these simulations for an emission based scheme with realistic state-of-the-art parameters and one with near-future parameters. The performance of these two regimes can be seen in table 4.4.

Parameter \ Regime	Realistic	Near Future
F	89.7%	95.3%
P_{success}	0.01%	10%
t_g^{eff}	$6\mu s$	$6\mu s$

Table 4.4: Performance of the emission based protocol for realistic state-of-the-art and near-future implementations [60, 61, 62, 63, 64].

The simulations are Monte-Carlo experiments that take as an input the effective gate time t_g^{eff}, the probability of success P_{success} and the actual density matrix of the Bell pair. We used a supercomputer [65] to perform these simulations as they take into consideration a decoherence model, which greatly increases the overhead as well as the accuracy of the simulation.

The decoherence that is taken into consideration is described by the relaxation times T_1 and T_2, which describe the minimum lifetime of the quantum state. The process T_1 is a *generalized amplitude damping* channel, which is a noise model that describes dissipation in an environment of finite temperature and entails loss of quantum information due to exchange of energy with the environment. Because the environment is assumed to be of much higher temperature than the energy splitting of the spin states, for $t \to \infty$ the state will be maximally mixed. The process T_2 is a *phase damping* channel, and it corresponds to loss of quantum information without loss of energy [10]. These values are fixed and different for the nuclear-spin-memory qubit and for the electronic-spin qubit. Also, there is a discrimination between idling relaxation time and the linking relaxation time. The linking relaxation time applies to the nuclear spin only, and it describes the noise induced on it by the entanglement creation sequence of the electronic spins. The values of the relaxation times can be found in table 4.5.

Relaxation time \ Qubit	Nuclear spin (Memory)	Electronic spin
$T_{1,\text{idle}}$	$300s$	∞
$T_{1,\text{link}}$	$0.03s$	N.A.
$T_{2,\text{idle}}$	$10s$	$1s$
$T_{2,\text{link}}$	$7.5ms$	N.A.

Table 4.5: Performance of the emission based protocol for realistic state-of-the-art and near-future implementations [54].

Now that we have defined our simulation setting with tables 4.2 and 4.5, we can compare the performance of the emission based (EB) protocol states from table 4.4 and the hardware-constrained entangling gate states (NEB) from figure 4.3. For this purpose we use the software found in [66]. The results can be seen in figure 4.4.

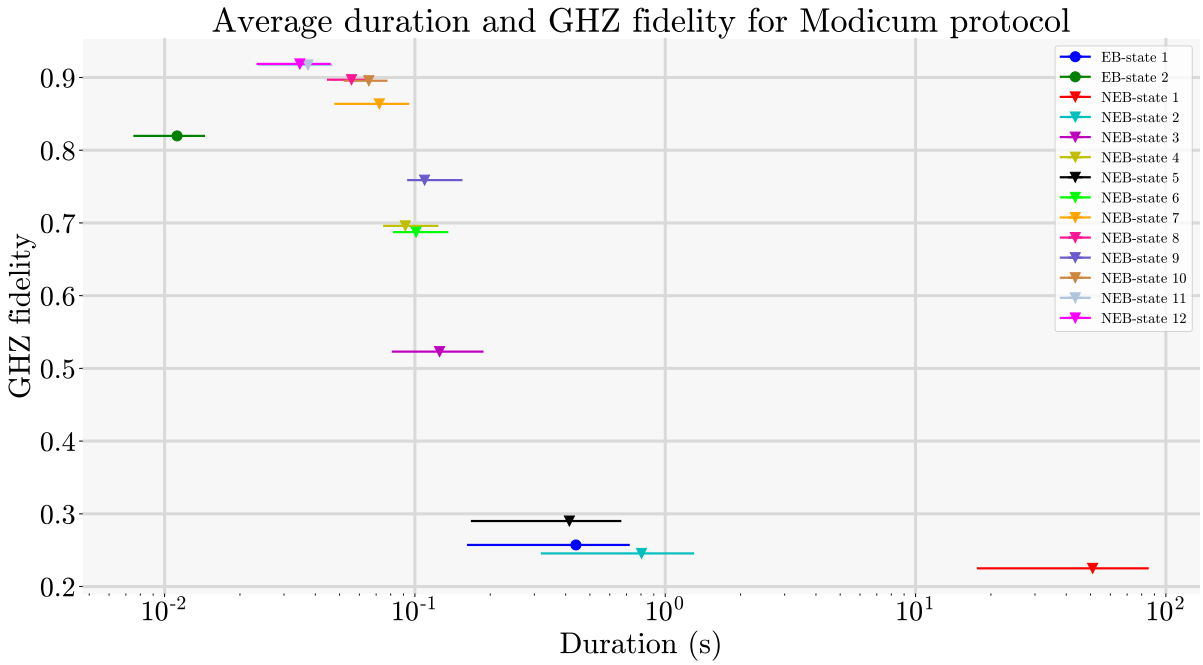

Figure 4.4: Performance of the emission (EB) and non-emission based (NEB) protocols when creating 4-GHZ states using the Modicum protocol for $5 \cdot 10^4$ Monte Carlo experiments. Duration is the time needed to generate the GHZ state. The horizontal error bars correspond to the 68.2% temporal interval of confidence. The NEB protocols are from the settings of figure 4.3 with the numbering from left to right and top to bottom.

Firstly, let us focus on the entangling gate states (NEB states). If we refer to figure 4.3, we shall realize that the lower the cost function was, the better the performance[5] is. Actually, the performance is a strictly decreasing function of the cost. From that we can conclude that our heuristically derived cost function was indeed appropriately selected.

Comparing the two protocols, we can see that NEB states 1 and 2 performed clearly worse than the state-of-the-art EB state, while the rest outperformed it. Those two correspond to the hardware constraints $\Delta_\gamma \in [3, 5]$ and $\eta = 0.9$. However, all of those states completely fail as their output fidelity is too low, as a result of the extreme effect of decoherence. This in turn, is caused by the long waiting times due to low probabilities of success.

Looking at the best performing states with GHZ fidelity above 0.8, we can see a separation between the qualities of the two protocols. It seems that the EB scheme provided faster GHZ generation but at the cost of fidelity. We can see that the top contestants for the NEB scheme were all protocols with a cost function below -200 from figure 4.3 and required roughly an optical separation $\Delta_{\max} \geq 10\gamma$ and a coupling efficiency $\eta \geq 0.95$.

[5]Performance improves as the GHZ fidelity increases and the duration needed to create the GHZ state decreases. So, the best performance lies on the top-left of the plot.

5

Discussion

Having concluded our work, we proceed to discuss our results and methods. It is important that some things are clear, and that we manage our expectations accordingly. We shall go into these remarks one-by-one.

Multi-qubit entangling gates
Our work had as a byproduct the definition of quasi-symmetric Hamiltonians. These Hamiltonians, although they can theoretically realize entangling gates for direct GHZ generation, we do not actually know with what overhead this comes. We know the number of conditions that need to be satisfied but the cost of satisfying them is not quite clear. Regardless, it might be interesting to try and engineer a Hamiltonian that could generate those gates using cavity or circuit quantum electrodynamics. Noteworthy though is that this is a general theoretical result and should not be confused with our proposed protocol. It is just that our protocol, for some connectivity, falls in this category.

Accuracy of gate description
The model that we developed for the protocol was inspired by realistic constraints. However, we do not know what other limitations arise by actually implementing it. It might be the case that we overlooked experimental constraints that render this gate inefficient and suboptimal. Additional interactions may need to be accounted for.

Parameter mixing of experimental implementations
Regarding the numerical results, one should be very careful as well. Throughout this work we used parameters from multiple prospective implementations of distributed architectures. The gate optimization was done primarily with a combination of SiV and SnV center parameters while the GHZ creation was modelled with NV center architecture parameters. Yet, each hardware is characterized by different parameter regimes and state-of-the-art performance metrics. As a result, we cannot draw any strong conclusions, even if our description of the gate does not overlook anything.

Tuning precision and adiabaticity
When dealing with numerics, it was assumed implicitly that everything can be tuned up to the float-precision of 15 significant digits. Of course, in realistic setups one should consider how well those parameters can actually be tuned and what implications this could have for the gate. For example, tuning the cavity-atom cooperativity may be quite challenging and cause the coupling efficiency to be altered as well. Moreover, the regimes we assumed were not thoroughly examined for adiabatic errors, although one would expect that they should be sufficiently low due to our selections and the previous work of Borregaard et al. (2015) [2]. In case that the adiabatic error is in fact too low, it might be worth it to compromise it to obtain a shorter gate time.

Simulations projection into the future
For all the GHZ creation simulations, the same timescale was assumed for the rest of the operations. This is quite unrealistic and leads to potentially counter-intuitive results. For example, if we were to

allow for an extremely high cooperativity and unconstrained optical separation, our gate would be perfect and instantaneous. Still though, the temporal interval of confidence would be $t_{0.99} > 1.5ms$ which is the needed time to perform SWAP gates. Instead, those values should also improve, at least with some heuristic, when projecting into the future regimes.

Comparing the two protocols
The comparison that we made between the two protocols was more of a proof of concept and should be considered with caution. We simulated both the emission based and integrated protocol with the same framework settings by merely switching the density matrices, probabilities of success and time needed for entanglement attempt, which is an approximation that should be further refined. The two protocols have different hardware requirements and the equivalency between the parameters of the two schemes is by no means trivial.

Also, as we saw from the results, the two protocols for future-projected parameters performed *differently* and not one better than the other. To draw comparative results, the tuple of average fidelity and time to create the GHZ state should be substituted by a single performance metric that better encapsulates the efficiency when measuring stabilizers.

Another branching point has to do with the GHZ creation protocols. We described two simple such protocols and proceeded to obtain results for the more elaborate of the two, namely *Modicum*. This barely scratches the surface though, as there are countless ways that a GHZ state can be created with intermediate distillation steps. As a result, the optimal protocol will be probably state dependent, and we would need to find it for both schemes.

Cost function definition
The definition of the cost function was proven to be appropriate as the performance was a decreasing function of the cost. Nevertheless, this does not mean that the optimal performance was achieved for each set of constraints. Running full scale optimization will probably not be feasible as the GHZ generation simulations required the use of a supercomputer. Instead, a better cost function should be considered for different GHZ protocols, potentially by tweaking the fidelity cap.

Fixing the incorrect timescale
As mentioned in section 4.3, the timescale is defined by the value of $1/\gamma$. We performed all the optimizations by selecting γ = 30MHz, but we missed a factor of 2π in comparison to experimentally achieved values. This means that we could in fact achieve for the same gate time, better probability of success and thus better overall performance for all parameter regimes.

Integrated Gate Protocol
Another very important aspect of the proposed protocol which was not elaborated on, is the fact that it is actually an integrated gate. This means that the modular quantum computer architecture can be more homogeneous. There is no need for a beam splitter setup to establish entanglement between nodes. Instead, an extra node has to be added in between that will be driven externally and measured afterwards to determine the success.

Moreover, in the high cooperativity limit maybe the need for distillation steps can be eliminated, as well as the need to store the state in the quantum memory. In such a regime that high probabilities of success will be possible, the gate can be run sequentially without worrying about the p^3 probability of success. This would alleviate the time-consuming process of switching the Bell pairs into the quantum memory, if this proves to be a temporal bottleneck at some point. That could potentially be achieved by activating and deactivating sequentially the connections of an auxiliary node among 4 qubit nodes, as

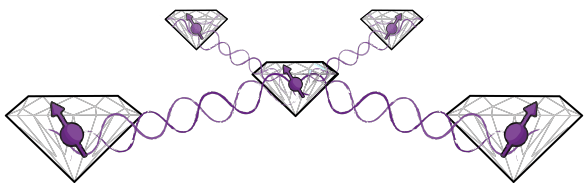

Figure 5.1: Architecture of 5 nodes where the central one acts as an auxiliary node [67].

seen in figure 5.1. One may notice that this architecture is identical to surface codes on superconducting circuits. The difference is that in the superconducting circuits the central nodes are auxiliary qubits where the stabilizer measurement is being carried out, while in the distributed computer paradigm they are used to generate a GHZ state that will be shared among the surrounding nodes. For low cooperativities this might not be an ideal architecture as it forbids the parallel creation of Bell pairs, which is critical in order to achieve high fidelity while using lower fidelity Bell pairs.

Future outlook
The accomplishment of this project is not that we simulated this protocol's performance for realistic setups. Rather we showcased that we can approximate its behavior for different regimes in a progressive manner. Experimentally trying to implement this scheme has the potential to reveal a lot of its limitations and potential edge while elaborating on the theoretical modelling of the scheme. Any additional considerations can easily be added into the framework that we have developed and improve the quality of the simulations. In fact, all previous paragraphs of this chapter contain prospective branching points of this project's future that could better outline this gate's potential.

6

Conclusion

In this work we investigated an entangling gate with the end goal of creating high fidelity GHZ states among nodes of distributed architectures. We expanded the intracavity protocol of Borregaard et al. (2015) [2] in two ways. A distributed paradigm was followed by separating the atoms into separate cavities that are connected by fibers. Moreover, we allowed both qubit ground states to couple to the cavity, which is motivated by electronic structures of SnV and SiV centers.

The separation of the atoms in cavities can be done following many geometries, leading to many possibilities. For this reason, we developed a customizable and versatile Python framework to solve analytically the adiabatic dynamics of this system based on the effective operator formalism for open systems introduced by Reiter and Sørensen (2012) [3]. This allows for easy definition of new interactions and geometries of architecture, while producing results swiftly and reliably.

Looking into the symmetry of these setups and fueled by the motivation of the GHZ state generation, we found a specific architecture which allows for the creation of a 3-partite GHZ state with a single entangling unitary CZ^2. We proceeded to generalize our results for any multi-qubit Hamiltonian that is *quasi-symmetric*, i.e. there is no discrimination of excitations among all but one qubits. These quasi-symmetric Hamiltonians can generate a CZ^N gate so long as it is appropriately tuned to satisfy $2N - 2$ extra conditions.

Our framework was used to obtain analytical results for a particular case of a CZ gate, `0-x-0`, where the qubit atoms are the same and symmetrically connected to the auxiliary cavity-atom system. We presented some refined expressions for the effective Hamiltonian and some loss rates. Using these expressions, we found out that there is a particular regime of parameters which ensures the scalability of the scheme, all while preserving low adiabatic errors. The scalability was also shown numerically as all the performance error metrics scaled with the cooperativity C as $1/\sqrt{C}$.

Next, we proceeded to optimize the gate with the end-goal of creating GHZ states. The optimization was done in a general parameter regime that we defined to ensure adiabaticity, under some hardware constraints inspired by realistic values. The optimization resulted in an appropriate tuning for each set of constraints. To this end, we also incorporated higher level parameters from NV center architectures, such that any potential bottlenecks are accounted for.

Having obtained the optimized gates, we went on to simulate the GHZ creation protocol Modicum [4] for these gates and two emission based schemes. From the results we got an indication of the hardware constraints that need to be satisfied in the future to have comparable performance between the two protocols. Additionally, we found out that our heuristically defined loss function was a decreasing function of the gate performance, thus showcasing its suitability.

Finally, we discussed our results and presented many potential avenues this project could be expanded. These include engineering of quasi-symmetric Hamiltonians for GHZ generation, more realistic Hamiltonian modelling and parameter regimes, accounting for imperfect tunings and adiabatic errors, refining the comparison between entangling schemes and fixing the timescale error we have made in the selection of γ. Lastly, some possible compact architecture is envisioned that could in the near or long term improve homogeneity and compactness of the architecture.

References

[1] Naomi H. Nickerson, Ying Li, and Simon C. Benjamin. "Topological quantum computing with a very noisy network and local error rates approaching one percent". In: *Nature Communications* 4.1 (Apr. 2013). DOI: 10.1038/ncomms2773. URL: https://doi.org/10.1038%2Fncomms2773.

[2] J. Borregaard et al. "Heralded Quantum Gates with Integrated Error Detection in Optical Cavities". In: *Phys. Rev. Lett.* 114 (11 Mar. 2015), p. 110502. DOI: 10.1103/PhysRevLett.114.110502. URL: https://link.aps.org/doi/10.1103/PhysRevLett.114.110502.

[3] Florentin Reiter and Anders S. Sørensen. "Effective operator formalism for open quantum systems". In: *Physical Review A* 85.3 (Mar. 2012). ISSN: 1094-1622. DOI: 10.1103/physreva.85.032111. URL: http://dx.doi.org/10.1103/PhysRevA.85.032111.

[4] Sebastian de Bone et al. "Protocols for Creating and Distilling Multipartite GHZ States With Bell Pairs". In: *IEEE Transactions on Quantum Engineering* 1 (2020), pp. 1–10. DOI: 10.1109/TQE.2020.3044179.

[5] Richard P. Feynman. "Simulating physics with computers". In: *International Journal of Theoretical Physics* 21.6 (June 1, 1982), pp. 467–488. ISSN: 1572-9575. DOI: 10.1007/BF02650179. URL: https://doi.org/10.1007/BF02650179.

[6] Paul Benioff. "The computer as a physical system: A microscopic quantum mechanical Hamiltonian model of computers as represented by Turing machines". In: *Journal of Statistical Physics* 22.5 (May 1980), pp. 563–591. ISSN: 0022-4715, 1572-9613. DOI: 10.1007/BF01011339. URL: http://link.springer.com/10.1007/BF01011339 (visited on 05/26/2022).

[7] Paul Benioff. "Quantum mechanical hamiltonian models of turing machines". In: *Journal of Statistical Physics* 29.3 (Nov. 1982), pp. 515–546. ISSN: 0022-4715, 1572-9613. DOI: 10.1007/BF01342185. URL: http://link.springer.com/10.1007/BF01342185 (visited on 05/26/2022).

[8] Alan Mathison Turing et al. "On computable numbers, with an application to the Entscheidungsproblem". In: *J. of Math* 58.345-363 (1936), p. 5.

[9] D. Deutsch. "Quantum theory, the Church-Turing principle and the universal quantum computer". In: *Proceedings of the Royal Society of London Series A* 400.1818 (July 1985), pp. 97–117. DOI: 10.1098/rspa.1985.0070.

[10] Michael A. Nielsen and Isaac L. Chuang. *Quantum Computation and Quantum Information: 10th Anniversary Edition*. Cambridge University Press, 2011. ISBN: 9781107002173. URL: https://www.amazon.com/Quantum-Computation-Information-10th-Anniversary/dp/1107002176?SubscriptionId=AKIAIOBINVZYXZQZ2U3A&tag=chimbori05-20&linkCode=xm2&camp=2025&creative=165953&creativeASIN=1107002176.

[11] Adriano Barenco et al. "Elementary gates for quantum computation". In: *Phys. Rev. A* 52 (5 Nov. 1995), pp. 3457–3467. DOI: 10.1103/PhysRevA.52.3457. URL: https://link.aps.org/doi/10.1103/PhysRevA.52.3457.

[12] Richard P. Feynman. "Quantum mechanical computers". In: *Foundations of Physics* 16.6 (June 1, 1986), pp. 507–531. ISSN: 1572-9516. DOI: 10.1007/BF01886518. URL: https://doi.org/10.1007/BF01886518.

[13] P.W. Shor. "Algorithms for quantum computation: discrete logarithms and factoring". In: *Proceedings 35th Annual Symposium on Foundations of Computer Science*. 1994, pp. 124–134. DOI: 10.1109/SFCS.1994.365700.

[14] Frank Arute et al. "Quantum supremacy using a programmable superconducting processor". In: *Nature* 574.7779 (Oct. 24, 2019), pp. 505–510. ISSN: 0028-0836, 1476-4687. DOI: 10.1038/s41586-019-1666-5. URL: http://www.nature.com/articles/s41586-019-1666-5.

[15] J. I. Cirac et al. "Distributed Quantum Computation over Noisy Channels". In: *Physical Review A* 59.6 (June 1, 1999), pp. 4249–4254. ISSN: 1050-2947, 1094-1622. DOI: 10.1103/PhysRevA.59.4249. arXiv: quant-ph/9803017. URL: http://arxiv.org/abs/quant-ph/9803017 (visited on 05/27/2022).

[16] Lov K. Grover. "Quantum Telecomputation". In: 1997.

[17] William K. Wootters and Wojciech Zurek. "A single quantum cannot be cloned". In: *Nature* 299 (1982), pp. 802–803.

[18] Daniel Gottesman. *Stabilizer Codes and Quantum Error Correction*. 1997. DOI: 10.48550/ARXIV.QUANT-PH/9705052. URL: https://arxiv.org/abs/quant-ph/9705052.

[19] S. B. Bravyi and A. Yu. Kitaev. *Quantum codes on a lattice with boundary*. 1998. DOI: 10.48550/ARXIV.QUANT-PH/9811052. URL: https://arxiv.org/abs/quant-ph/9811052.

[20] Daniel M. Greenberger, Michael A. Horne, and Anton Zeilinger. "Going Beyond Bell's Theorem". In: (2007). DOI: 10.48550/ARXIV.0712.0921. URL: https://arxiv.org/abs/0712.0921.

[21] Matthew E. Trusheim et al. "Transform-Limited Photons From a Coherent Tin-Vacancy Spin in Diamond". In: *Physical Review Letters* 124.2 (Jan. 14, 2020), p. 023602. ISSN: 0031-9007, 1079-7114. DOI: 10.1103/PhysRevLett.124.023602. URL: https://link.aps.org/doi/10.1103/PhysRevLett.124.023602 (visited on 05/22/2022).

[22] Notes by: L. Childress on Lectures by M.D. Lukin. *Modern Atomic and Optical Physics II*. Fall 2005.

[23] Mark Fox. *Quantum optics: an introduction*. Oxford Master Series in Physics, 6. Oxford University Press, USA, 2006. ISBN: 0198566735; 9780198566731; 9781435606807; 1435606809.

[24] Joseph H. Eberly Leslie Allen. *Optical resonance and two-level atoms*. Interscience monographs and texts in physics and astronomy, 28. Wiley, 1975. ISBN: 0471023272; 9780471023272.

[25] Jim Napolitano J. J. Sakurai. *Modern Quantum Mechanics*. 3rd ed. Cambridge University Press, 2020. ISBN: 9781108473224; 1108473229.

[26] Gilbert Grynberg Claude Cohen-Tannoudji Jacques Dupont-Roc. *Atom-photon interactions: basic processes and applications*. Wiley. Wiley Science Paperback Series. Wiley-VCH, 1998. ISBN: 0471293369; 9780471293361.

[27] Murray Sargent Pierre Meystre. *Elements of Quantum Optics*. 4th ed. Springer, 2007. ISBN: 3540742093; 9783540742098.

[28] E Brion, L H Pedersen, and K Mølmer. "Adiabatic elimination in a lambda system". In: *Journal of Physics A: Mathematical and Theoretical* 40.5 (Jan. 2007), pp. 1033–1043. ISSN: 1751-8121. DOI: 10.1088/1751-8113/40/5/011. URL: http://dx.doi.org/10.1088/1751-8113/40/5/011.

[29] Klaus Mølmer, Yvan Castin, and Jean Dalibard. "Monte Carlo wave-function method in quantum optics". In: *J. Opt. Soc. Am. B* 10.3 (Mar. 1993), pp. 524–538. DOI: 10.1364/JOSAB.10.000524. URL: http://opg.optica.org/josab/abstract.cfm?URI=josab-10-3-524.

[30] G. Lindblad. "On the generators of quantum dynamical semigroups". In: *Communications in Mathematical Physics* 48.2 (1976), pp. 119–130. DOI: cmp/1103899849. URL: https://doi.org/.

[31] Vittorio Gorini, Andrzej Kossakowski, and E. C. G. Sudarshan. "Completely positive dynamical semigroups of N-level systems". In: *Journal of Mathematical Physics* 17.5 (1976), pp. 821–825. DOI: 10.1063/1.522979. eprint: https://aip.scitation.org/doi/pdf/10.1063/1.522979. URL: https://aip.scitation.org/doi/abs/10.1063/1.522979.

[32] Joschka Roffe. "Quantum error correction: an introductory guide". In: *Contemporary Physics* 60.3 (2019), pp. 226–245. DOI: 10.1080/00107514.2019.1667078. eprint: https://doi.org/10.1080/00107514.2019.1667078. URL: https://doi.org/10.1080/00107514.2019.1667078.

[33] P.F.W. Möller. "Modelling the performance of a distributed surface code in presence of decoherence". MA thesis. Delft University of Technology, 2021.

[34] Daniel Gottesman. "The Heisenberg Representation of Quantum Computers". In: (1998). DOI: 10.48550/ARXIV.QUANT-PH/9807006. URL: https://arxiv.org/abs/quant-ph/9807006.

[35] A. Yu. Kitaev. "Quantum Error Correction with Imperfect Gates". In: *Quantum Communication, Computing, and Measurement*. Ed. by O. Hirota, A. S. Holevo, and C. M. Caves. Boston, MA: Springer US, 1997, pp. 181–188. ISBN: 978-1-4615-5923-8. DOI: 10.1007/978-1-4615-5923-8_19. URL: https://doi.org/10.1007/978-1-4615-5923-8_19.

[36] A.Yu. Kitaev. "Fault-tolerant quantum computation by anyons". In: *Annals of Physics* 303.1 (2003), pp. 2–30. ISSN: 0003-4916. DOI: https://doi.org/10.1016/S0003-4916(02)00018-0. URL: https://www.sciencedirect.com/science/article/pii/S0003491602000180.

[37] Chai Jing Hao. "Assessing Fault-Tolerance Conditions for Surface Code Implemented With Noisy Devices". PhD thesis. Centre for Quantum Technologies, National University of Singapore, 2020.

[38] Naomi H. Nickerson, Joseph F. Fitzsimons, and Simon C. Benjamin. "Freely Scalable Quantum Technologies Using Cells of 5-to-50 Qubits with Very Lossy and Noisy Photonic Links". In: *Physical Review X* 4.4 (Dec. 9, 2014), p. 041041. ISSN: 2160-3308. DOI: 10.1103/PhysRevX.4.041041. URL: https://link.aps.org/doi/10.1103/PhysRevX.4.041041 (visited on 05/27/2022).

[39] T. Pellizzari. "Quantum Networking with Optical Fibres". In: *Physical Review Letters* 79.26 (Dec. 1997), pp. 5242–5245. DOI: 10.1103/physrevlett.79.5242. URL: https://doi.org/10.1103%2Fphysrevlett.79.5242.

[40] Alessio Serafini, Stefano Mancini, and Sougato Bose. "Distributed Quantum Computation via Optical Fibers". In: *Phys. Rev. Lett.* 96 (1 Jan. 2006), p. 010503. DOI: 10.1103/PhysRevLett.96.010503. URL: https://link.aps.org/doi/10.1103/PhysRevLett.96.010503.

[41] Shinya Kato et al. "Observation of dressed states of distant atoms with delocalized photons in coupled-cavities quantum electrodynamics". In: *Nature Communications* 10.1 (Dec. 2019), p. 1160. ISSN: 2041-1723. DOI: 10.1038/s41467-019-08975-8. URL: http://www.nature.com/articles/s41467-019-08975-8 (visited on 05/07/2022).

[42] M. K. Bhaskar et al. "Experimental demonstration of memory-enhanced quantum communication". In: *Nature* 580.7801 (Apr. 2, 2020), pp. 60–64. ISSN: 0028-0836, 1476-4687. DOI: 10.1038/s41586-020-2103-5. URL: http://www.nature.com/articles/s41586-020-2103-5 (visited on 05/23/2022).

[43] Guido Van Rossum and Fred L. Drake. *Python 3 Reference Manual*. Scotts Valley, CA: CreateSpace, 2009. ISBN: 1441412697.

[44] J.R. Johansson, P.D. Nation, and Franco Nori. "QuTiP 2: A Python framework for the dynamics of open quantum systems". In: *Computer Physics Communications* 184.4 (Apr. 1, 2013), pp. 1234–1240. ISSN: 0010-4655. DOI: 10.1016/j.cpc.2012.11.019. URL: https://www.sciencedirect.com/science/article/pii/S0010465512003955.

[45] Inc. Wolfram Research. *Mathematica, Version 12.0*. Champaign, IL, 2019.

[46] The SageMath Developers. *sagemath/sage: 9.5*. Version 9.5. Jan. 2022. DOI: 10.5281/zenodo.6259615. URL: https://doi.org/10.5281/zenodo.6259615.

[47] Alastair Kay. *Quantikz*. 2019. DOI: 10.17637/RH.7000520. URL: https://royalholloway.figshare.com/articles/Quantikz/7000520.

[48] Simon Groeblacher et al. "Highly efficient coupling from an optical fiber to a nanoscale silicon optomechanical cavity". In: *Applied Physics Letters* 103.18 (Oct. 28, 2013), p. 181104. ISSN: 0003-6951, 1077-3118. DOI: 10.1063/1.4826924. arXiv: 1309.1181[cond-mat,physics:physics,physics:quant-ph]. URL: http://arxiv.org/abs/1309.1181 (visited on 05/22/2022).

[49] John Preskill. *Quantum Computation course, Lecture Notes*. 2022.

[50] Shahriar Aghaeimeibodi et al. "A nanophotonic interface for tin-vacancy spin qubits in diamond". In: *Quantum Nanophotonic Materials, Devices, and Systems 2021*. Quantum Nanophotonic Materials, Devices, and Systems 2021. Ed. by Mario Agio, Cesare Soci, and Matthew T. Sheldon. San Diego, United States: SPIE, Aug. 1, 2021, p. 10. ISBN: 978-1-5106-4450-2 978-1-5106-4451-9. DOI: 10.1117/12.2593984. URL: https://www.spiedigitallibrary.org/conference-proceedings-of-spie/11806/2593984/A-nanophotonic-interface-for-tin-vacancy-spin-qubits-in-diamond/10.1117/12.2593984.full (visited on 05/22/2022).

[51] Alison E. Rugar et al. "Narrow-linewidth tin-vacancy centers in a diamond waveguide". In: *ACS Photonics* 7.9 (Sept. 16, 2020), pp. 2356–2361. ISSN: 2330-4022, 2330-4022. DOI: 10.1021/acsphotonics.0c00833. arXiv: 2005.10385[cond-mat,physics:physics,physics:quant-ph]. URL: http://arxiv.org/abs/2005.10385 (visited on 05/22/2022).

[52] Kazuhiro Kuruma et al. "Coupling of a single tin-vacancy center to a photonic crystal cavity in diamond". In: *Applied Physics Letters* 118.23 (June 7, 2021), p. 230601. ISSN: 0003-6951, 1077-3118. DOI: 10.1063/5.0051675. URL: https://aip.scitation.org/doi/10.1063/5.0051675 (visited on 05/23/2022).

[53] J. D. Hunter. "Matplotlib: A 2D graphics environment". In: *Computing in Science & Engineering* 9.3 (2007), pp. 90–95. DOI: 10.1109/MCSE.2007.55.

[54] C. E. Bradley et al. *Robust quantum-network memory based on spin qubits in isotopically engineered diamond*. Number: arXiv:2111.09772. Nov. 18, 2021. arXiv: 2111.09772[cond-mat,physics:quant-ph]. URL: http://arxiv.org/abs/2111.09772 (visited on 05/27/2022).

[55] Rainer Storn and Kenneth Price. "Differential Evolution - A Simple and Efficient Heuristic for Global Optimization over Continuous Spaces". In: *Journal of Global Optimization* 11 (Jan. 1997), pp. 341–359. DOI: 10.1023/A:1008202821328.

[56] Pauli Virtanen et al. "SciPy 1.0: Fundamental Algorithms for Scientific Computing in Python". In: *Nature Methods* 17 (2020), pp. 261–272. DOI: 10.1038/s41592-019-0686-2.

[57] Richard H. Byrd et al. "A limited memory algorithm for bound constrained optimization". English. In: *SIAM Journal of Scientific Computing* 16 (Sept. 1995), pp. 1190–1208. ISSN: 1064-8275. DOI: 10.1137/0916069.

[58] Ciyou Zhu et al. "Algorithm 778: L-BFGS-B: Fortran Subroutines for Large-Scale Bound-Constrained Optimization". In: *ACM Trans. Math. Softw.* 23.4 (Dec. 1997), pp. 550–560. ISSN: 0098-3500. DOI: 10.1145/279232.279236. URL: https://doi.org/10.1145/279232.279236.

[59] Michael L. Waskom. "seaborn: statistical data visualization". In: *Journal of Open Source Software* 6.60 (2021), p. 3021. DOI: 10.21105/joss.03021. URL: https://doi.org/10.21105/joss.03021.

[60] M. Pompili et al. "Realization of a multinode quantum network of remote solid-state qubits". In: *Science* 372.6539 (2021), pp. 259–264. DOI: 10.1126/science.abg1919. eprint: https://www.science.org/doi/pdf/10.1126/science.abg1919. URL: https://www.science.org/doi/abs/10.1126/science.abg1919.

[61] Filip Rozpędek et al. "Near-term quantum-repeater experiments with nitrogen-vacancy centers: Overcoming the limitations of direct transmission". In: *Phys. Rev. A* 99 (5 May 2019), p. 052330. DOI: 10.1103/PhysRevA.99.052330. URL: https://link.aps.org/doi/10.1103/PhysRevA.99.052330.

[62] Tim Coopmans et al. "NetSquid, a NETwork Simulator for QUantum Information using Discrete events". In: *Communications Physics* 4.1 (Dec. 2021), p. 164. ISSN: 2399-3650. DOI: 10.1038/s42005-021-00647-8. URL: http://www.nature.com/articles/s42005-021-00647-8 (visited on 05/31/2022).

[63] Axel Dahlberg et al. "A link layer protocol for quantum networks". In: *Proceedings of the ACM Special Interest Group on Data Communication*. SIGCOMM '19: ACM SIGCOMM 2019 Conference. Beijing China: ACM, Aug. 19, 2019, pp. 159–173. ISBN: 978-1-4503-5956-6. DOI: 10.1145/3341302.3342070. URL: https://dl.acm.org/doi/10.1145/3341302.3342070 (visited on 05/31/2022).

[64] Peter C. Humphreys et al. "Deterministic delivery of remote entanglement on a quantum network". In: *Nature* 558.7709 (June 2018), pp. 268–273. ISSN: 0028-0836, 1476-4687. DOI: 10.1038/s41586-018-0200-5. URL: http://www.nature.com/articles/s41586-018-0200-5 (visited on 05/31/2022).

[65] *This work was carried out on the Dutch national e-infrastructure with the support of SURF Cooperative.*

[66] GitHub repository. *Open Surface code Simulations*. URL: https://github.com/Poeloe/oop_surface_code/tree/auto_generated_GHZ_prots.

[67] Adapatation of picture in QuTech blog. URL: https://blog.qutech.nl/2018/11/26/how-can-we-speed-up-the-%20quantum-internet/.

Code

The code used to obtain analytically the dynamics in the effective operator formalism and the optimization of the gates can be found at: https://github.com/yorgossot/modular_effective_operator.git